



# 3D Seismic reflection evidence for lower crustal intrusions beneath the Faroe–Shetland Basin, NE Atlantic Margin

Lucinda K. Layfield<sup>1</sup>, Nick Schofield<sup>1\*</sup>, Douglas Watson<sup>1</sup>, Simon P. Holford<sup>2</sup>, David W. Jolley<sup>1</sup>, Ben A. Kilhams<sup>1</sup>, David K. Muirhead<sup>1</sup>, Alan M. Roberts<sup>3</sup>, Andrew D. Alvey<sup>3</sup>, Alex Ellwood<sup>4</sup> and Mike Widdowson<sup>5</sup>


<sup>1</sup> Department of Geology and Geophysics, University of Aberdeen, Aberdeen AB24 3EU, UK

<sup>2</sup> Australian School of Petroleum, University of Adelaide, Adelaide, South Australia, Australia

<sup>3</sup> Badley Geoscience Ltd., North Beck House, North Beck Lane, Spilsby, Lincolnshire PE23 5NB, UK

<sup>4</sup> Schlumberger Ltd, Schlumberger House, Buckingham Gate, Gatwick, West Sussex RH6 0NZ, UK

<sup>5</sup> School of Environmental Sciences, University of Hull, Hull HU6 7RX, UK

 LKL, 0000-0002-5693-4959; DW, 0000-0001-9575-3141; SPH, 0000-0002-4524-8822; DWJ, 0000-0003-0909-2952; BAK, 0000-0002-4444-6800; DKM, 0000-0003-2065-6042; AMR, 0000-0003-4839-0741; MW, 0000-0002-8522-0138

\*Correspondence: [n.schofield@abdn.ac.uk](mailto:n.schofield@abdn.ac.uk)

**Abstract:** Lower crustal intrusion is considered to be a common process along volcanic or magma-rich passive margins, including the NE Atlantic Margin, where it is thought to have occurred during phases of Paleogene magmatism, both prior to and during continental break-up between NW Europe and Greenland. Evidence of Paleogene magmatism is prevalent throughout the sub-basins of the Faroe–Shetland Basin as extensive lava flows and pervasive suites of igneous intrusions. However, in contrast with other areas located along the NE Atlantic Margin, no lower crustal reflectivity indicative of lower crustal intrusion has been documented beneath the Faroe–Shetland Basin. The nearest documentation of lower crustal reflectivity and interpretation of lower crustal intrusion to the Faroe–Shetland Basin is NW of the Fugloy Ridge, beneath the Norwegian Basin of the Faroese sector. Despite this, the addition of magma within the lower crust and/or at the Mohorovičić discontinuity is thought to have played a part in Paleogene uplift and the subsequent deposition of Paleocene–Eocene sequences. Advances in sub-basalt seismic acquisition and processing have made significant improvements in facilitating the imaging of deep crustal structures along the NE Atlantic Margin. This study used broadband 3D seismic reflection data to map a series of deep (*c.* 14–20 km depth) high-amplitude reflections that may represent igneous intrusions within the lower crust beneath the central-northern Corona Ridge. We estimate that the cumulative thicknesses of the reflections may be >5 km in places, which is consistent with published values of magmatic underplating within the region based on geochemical and petrological data. We also estimate that the total volume of lower crustal high-amplitude reflections within the 3D dataset may be >2000 km<sup>3</sup>. 2D gravity modelling of a seismic line located along the central-northern Corona Ridge supports the interpretation of lower crustal intrusions beneath this area. This study provides evidence of a potential mechanism for Paleogene uplift within the region. If uplift occurred as a result of lower crustal intrusions emplaced within the crust during the Paleogene, then we estimate that *c.* 300 m of uplift may have been generated within the Corona Ridge area.

Received 7 December 2022; revised 30 April 2023; accepted 22 May 2023

The addition of magma within the lower crust or at the Mohorovičić discontinuity (Moho), commonly termed magmatic underplating (Cox 1980, 1993; White and McKenzie 1989*a, b*), is considered to be a common process associated with continental rifting and the development of volcanic or magma-rich passive margins, such as the NE Atlantic Margin (Geoffroy 2005; Thybo and Artemieva 2013; Ernst 2014; Lang *et al.* 2020). Within large igneous provinces, including the North Atlantic Igneous Province (NAIP), a large proportion of the magma generated during periods of magmatism is hypothesized to have solidified at the Moho or to have been emplaced as igneous intrusions within the lower crust (Cox 1980, 1993; White and McKenzie 1989*a, b*; White 1992; Ernst 2014; Magee *et al.* 2018). Estimates by Cox (1993) for the Karoo province suggest that 30–40% of the magma volume may remain at the base of the lithosphere. However, the precise ratio of extrusive volcanism to magmatic underplating remains enigmatic and is unlikely to be uniform across different large igneous provinces due to variable crustal thicknesses and stress regimes (White *et al.* 2010).

During the Paleogene, prior to and during continental break-up between NW Europe and Greenland, significant volumes of magma

are thought to have been generated within the mantle and propagated through the stretched and thinned continental crust to be emplaced within existing sedimentary successions along the NE Atlantic Margin, both as igneous intrusions and erupted onto the surface as flood basalts, forming part of the NAIP (Cox 1980; White *et al.* 1987; White and McKenzie 1989*b*; Smallwood *et al.* 1999; Jolley and Bell 2002; Planke *et al.* 2005; Schofield *et al.* 2017; Jolley *et al.* 2021 and references cited therein). Within the Faroe–Shetland Basin (FSB), the emplacement of magma is thought to have been largely controlled by pre-existing basement-bounding faults within the continental crystalline basement (White and McKenzie 1989*b*; Trude 2004; Ellis *et al.* 2009; Schofield *et al.* 2017).

The detailed nature of the deep crustal parts of magma plumbing systems along magma-rich passive margins remains enigmatic. Prior to advances in seismic acquisition and processing, the internal reflective character of the lower crust along the NE Atlantic Margin was typically not resolved due to low seismic resolution and the poor signal-to-noise ratio at such depths. Subsequently, the possible presence of lower crustal intrusions was generally only detected as a high-velocity layer within refraction and velocity datasets along the NE Atlantic Margin (e.g. White *et al.* 1987; Richardson *et al.* 1998;

Mjelde *et al.* 2001, 2009). Consequently, it remained unknown whether the addition of magma within the lower crust and/or at the Moho consisted of large continuous volumes of magma (a thick layer of ultramafic rock at the Moho, previously referred to as magmatic underplating; Cox 1980), a series of intrusions (e.g. Abdelmalak *et al.* 2017), or if the nature of this magmatic source varied depending on whether emplacement was beneath and/or within continental or magmatic crust (Thybo and Artemieva 2013; Thybo *et al.* 2013). More recent work focused along the NE Atlantic Margin has suggested that the emplacement of igneous material within the lower crust may have occurred as a series of igneous intrusions that produced lower crustal reflectivity (see Smith *et al.* 2005; White *et al.* 2008, 2010; Abdelmalak *et al.* 2017; Wrona *et al.* 2019b), not as a continuous volume of magma as previously hypothesized (White and Smith 2009; Thybo *et al.* 2013).

The widespread presence of extensive flood basalts and igneous intrusions within the FSB, thought to be sourced from a deep crustal magma reservoir postulated to be beneath the region (Cox 1980, 1993; Clift 1991, 1997; Hansen *et al.* 2019), creates challenges for imaging deep crustal structures (Hardwick *et al.* 2010; Poppitt *et al.* 2018). The presence of igneous material within the lower crust and at the Moho beneath the FSB has hitherto only been inferred, despite being hypothesized as a potential mechanism for Paleogene uplift and the subsequent deposition of Paleocene–Eocene sequences within the NE Atlantic region (Brodie and White 1994, 1995; White 1997; White and Lovell 1997; Clift and Turner 1998; Naylor *et al.* 1999; Jones *et al.* 2002; MacLennan and Lovell 2002; Tiley *et al.* 2004; Rudge *et al.* 2008; Smallwood 2008).

We have used a broadband 3D seismic reflection dataset to map and identify a series of deep (*c.* 14–20 km depth) high-amplitude (high acoustic impedance contrast) reflections that may represent igneous intrusions within the lower crust and at the Moho beneath the central-northern Corona Ridge, providing evidence of a potential mechanism, speculated by previous workers, that may have generated Paleogene uplift. We also used a long-offset 2D seismic reflection line, the WesternGeco 2D iSIMM Faroes profile, to place our results in a regional context with the nearest interpretation of lower crustal intrusions to the FSB (the Norwegian Basin; Smith *et al.* 2005; White *et al.* 2008, 2010) and to place our results in the context of the broader NE Atlantic Margin.

## Geological history

The FSB is located along the NE Atlantic Margin (Fig. 1a) and is hosted within the inboard, rifted continental crust component of a magma-rich passive margin. The basin is situated between the Møre Basin to the NE and the Rockall Basin to the SW and consists of several smaller sub-basins separated by NE–SW-trending intra-basinal highs of Precambrian crystalline basement rock (Figs 1b, 2) (Hitchen and Ritchie 1987; Doré *et al.* 1997; Ritchie *et al.* 2011; Holdsworth *et al.* 2019). However, towards the West and North Shetland platforms, the basement composition changes from Precambrian crystalline rocks to Moine and Dalradian (Neoproterozoic) and Caledonian (Paleozoic) meta-sedimentary rocks (Kinny *et al.* 2005; Holdsworth *et al.* 2019; Layfield *et al.* 2022). The prominent NE–SW structural trend of the sedimentary sub-basins across the FSB is thought to have originated as Precambrian shear zones, which were later reactivated during the Caledonian Orogeny and subsequent Caledonian collapse in the Devonian (Moy and Imber 2009; Smith and Ziska 2011). These pre-existing structural fabrics have since been exploited throughout the complex structural evolution of the FSB during multiple phases of extension from the Permo-Triassic to the Paleocene (Doré *et al.* 1997, 1999; Ritchie *et al.* 2011; Ellis and Stoker 2014).

The proto-Atlantic rift system was active throughout the Permo-Triassic to Cretaceous, contributing to both the fragmentation of

Pangaea and, ultimately, the opening of the North Atlantic Ocean (Ellis and Stoker 2014; Stoker *et al.* 2017b). The earliest recognized rifting event within the FSB is thought to have occurred during the Permo-Triassic, resulting in the formation of several NE–SW-trending half-graben basins (Sørensen 2003; Stoker *et al.* 2017b). Renewed extension occurred during the Mid- to Late Jurassic, contemporaneous with the widespread establishment of rifting within the North Sea (Ritchie and Varming 2011; Ritchie *et al.* 2011). This was followed by post-rift thermal subsidence, which, coupled with a rise in global sea-level, initiated an early Jurassic marine incursion (Ritchie and Varming 2011; Layfield *et al.* 2022). A further phase of widespread extension commencing during the early Cretaceous largely contributed to the development of the contemporary basin structure, manifested at the present day within the FSB as sub-basins separated by intra-basinal highs (Ritchie *et al.* 2011; Stoker 2016; Hardman *et al.* 2018a; Layfield *et al.* 2022). Several phases of continued extension are thought to have occurred within the Cretaceous, followed by post-rift thermal subsidence (Larsen *et al.* 2010; Stoker and Ziska 2011; Stoker 2016). Post-rift thermal subsidence is thought to have been interrupted in the early Paleocene by a minor final rifting phase (Smallwood and Gill 2002).

The start of seafloor spreading between *c.* 56 and 55 Ma (Ellis and Stoker 2014; Stoker *et al.* 2017a, b; Jolley *et al.* 2021) resulted in the opening of the NE Atlantic Ocean (*sensu stricto*), leading to the separation of eastern Greenland from NW Europe (Ellis and Stoker 2014; Stoker *et al.* 2017a). Uplift commenced within the late Paleocene (*c.* 63 Ma; Hardman *et al.* 2018b). Paleogene uplift has been linked to the arrival of a thermal anomaly (see Nadin *et al.* 1997; Jones *et al.* 2002; Rudge *et al.* 2008; Shaw-Champion *et al.* 2008; Hartley *et al.* 2011; Fletcher *et al.* 2013; Hardman *et al.* 2018b), crustal thickening caused by the emplacement of magma within the lower crust and at the Moho (i.e. magmatic underplating) (MacLennan and Lovell 2002; Tiley *et al.* 2004) and changes in the tectonic regime (Ellis and Stoker 2014; Mudge 2015; Jolley *et al.* 2021). The Cenozoic subsidence of the FSB was punctuated by phases of inversion during the late Paleocene, early to mid-Eocene and Oligo-Miocene (Smallwood 2004; Ritchie *et al.* 2008; Ellis *et al.* 2009; Stoker *et al.* 2010).

## Paleogene magmatism within the FSB, NE Atlantic Margin

Coincident with the proposed arrival of a regional thermal anomaly beneath the region, commonly linked to the initiating proto-Icelandic mantle plume (Nadin *et al.* 1997; White 1997; White and Lovell 1997; Chambers and Fitton 2000; Jones *et al.* 2002; Rudge *et al.* 2008; Shaw-Champion *et al.* 2008; Hartley *et al.* 2011; Hardman *et al.* 2018b), the NE Atlantic region was subject to extensive magmatism throughout the Paleogene (Nadin *et al.* 1997; Jolley and Bell 2002; Schofield *et al.* 2017; Jolley *et al.* 2021). This magmatism resulted in the formation of the NAIP, which consists of widespread extrusive components, a series of volcanoclastic beds, including airfall tuffs, and an extensive suite of igneous intrusions (Jolley and Bell 2002; Passey and Hitchen 2011; Schofield *et al.* 2017; Watson *et al.* 2017). Extrusive volcanism is mainly expressed within the Faroe Islands Basalt Group, which records the eruption of series of thick flood basalt sequences initiated during the Thanetian at *c.* 57 Ma (Jolley *et al.* 2021) and thought to cover an area of *c.* 40 000 km<sup>2</sup> within the FSB (Jolley and Bell 2002; Passey and Bell 2007; Passey and Jolley 2009; Schofield *et al.* 2017). The Faroe–Shetland Sill Complex represents the intrusive component of this igneous activity within the FSB and is thought to cover a minimum area of *c.* 22 500 km<sup>2</sup> (Passey and Hitchen 2011; Schofield *et al.* 2017; Mark *et al.* 2018a, b). Despite this widespread evidence for Paleogene magmatism in the FSB, there is no published evidence of lower crustal seismic reflectivity



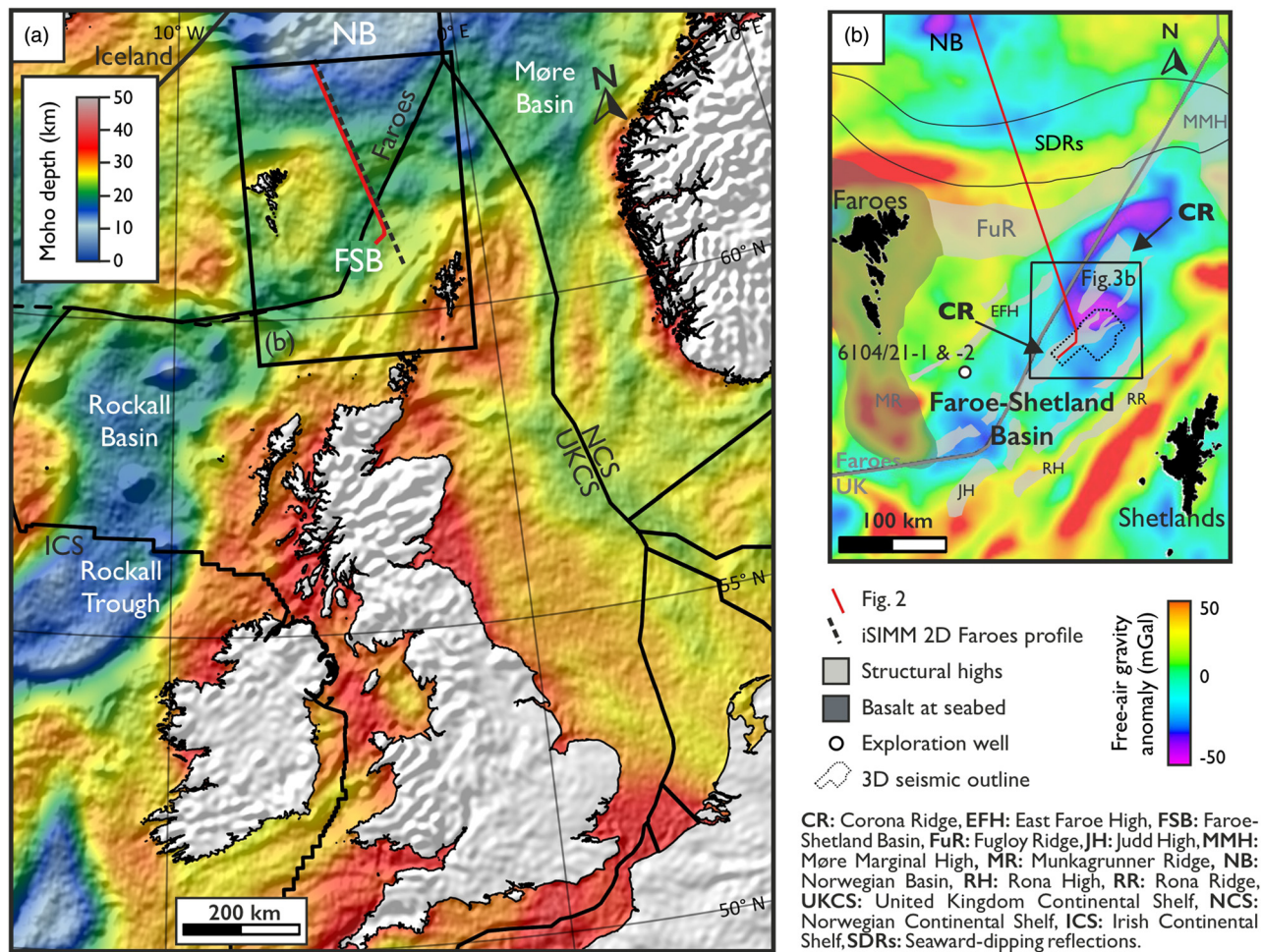


**Fig. 1.** (a) Moho depth map of the UK continental shelf, modified from [Badley Geoscience Limited \(2019\)](#); freely available from the North Sea Transition Authority Open Data site). The Moho depth map is based on model 2, which is considered to be the best case for the Atlantic Margin and uses a 35 km reference Moho depth, a 35 km initial crustal thickness and a normal magmatic addition of 7 km ([Badley Geoscience Limited 2019](#), p. 15). For the models within the OCTek-UK report, the Moho depth and total crustal thickness are unaffected by the amount of magmatic addition and a density for the crystalline crust of  $2850 \text{ kg m}^{-3}$  was used compared with  $2750 \text{ kg m}^{-3}$  used by this study for gravity modelling. The methods for determining Moho depth using 3D gravity inversion are described within the [Badley Geoscience Limited \(2019\)](#) OCTek-UK project, [Alvey \*et al.\* \(2008\)](#), [Chappell and Kuszniir \(2008\)](#) and [Kuszniir \*et al.\* \(2020\)](#). (b) Map showing free air gravity anomaly data of the Faroe–Shetland Basin area, the Galloway/Corona 3D seismic survey area (dashed line), the seismic line shown in [Figure 2](#) (red line), the key structural elements (grey), the seaward-dipping reflections from [Funk \*et al.\* \(2016\)](#) and the location of [Figure 3b](#) (black box). The intra-basinal highs (grey shapes) are from [Moy and Imber \(2009\)](#) and [Hardman \*et al.\* \(2018a\)](#) and the Corona Ridge is from [Layfield \*et al.\* \(2022\)](#). The free air gravity anomaly data are from the International Gravimetric Bureau World Gravity Map 2012 Global Model and are publicly available.

to support the presence of igneous material within the lower crust, which may have acted as a deep crustal magma reservoir for Paleogene magmatism ([Clift 1997](#); [Shaw-Champion \*et al.\* 2006, 2008](#); [Passey and Hitchen 2011](#); [Hansen \*et al.\* 2019](#)). The most proximal evidence of seismic reflectivity interpreted as lower crustal intrusions to the FSB was documented by [White \*et al.\* \(2008, 2010\)](#) beneath the Norwegian Basin ([Fig. 1](#)) to the east of the Faroe Islands (*c.* 160 km from the Corona Ridge), near to the continent–ocean transition.

## The Moho, magmatic underplating and lower crustal intrusions along the NE Atlantic Margin

### Constraints on the depth to the Moho

Based on seismic reflection, seismic refraction and gravity data, previous researchers have proposed that the depth to the Moho along the NE Atlantic Margin varies between 14 and 30 km (see [Gernigon \*et al.\* 2004](#); [McBride \*et al.\* 2004](#); [Raum \*et al.\* 2005](#); [Smith \*et al.\* 2005](#); [White \*et al.\* 2005](#); [Makris \*et al.\* 2009](#); [Ritchie \*et al.\*](#)

[2011](#); [Funk \*et al.\* 2014, 2016, 2017](#); [Petersen and Funk 2017](#); [Peron-Pinvidic \*et al.\* 2022](#)) and *c.* 9–13 s TWT ([Warner 1987](#)). Beneath the Corona Ridge, Moho depths are thought to lie towards the shallower end of these estimates, between 14 and 21 km ([Hughes \*et al.\* 1997](#); [Makris \*et al.\* 2009](#); [Ritchie \*et al.\* 2011](#); [Funk \*et al.\* 2016, 2017](#)). The Moho depth map ([Fig. 1a](#)) has been modified from the most recent series of published Moho depth maps from the OCTek-UK project ([Badley Geoscience Limited 2019](#)) and shows the Moho at *c.* 20 km depth in the Corona Ridge area. The crust thickens towards the northwestern (the Munkagranner and Fugloy ridges, [Fig. 1](#)) and southeastern (the West Shetland Platform) flanks of the FSB, where the depth to the Moho increases to between 25 and 30 km ([Fig. 1a](#)) ([Ritchie \*et al.\* 2011](#); [Rippington \*et al.\* 2015](#)). Beneath the central-northern Corona Ridge, the depth to the Moho is interpreted as between 14 and 20 km depth based on seismic refraction (the WesternGeco 2D iSIMM Faroes profile, [Fig. 2](#); [White \*et al.\* 2005](#); [Roberts \*et al.\* 2009](#)) and wide-angle reflection (the Faeroer-93 profiles I and II; [Makris \*et al.\* 2009](#)) data and, within the 3D seismic data, is interpreted at the base of the high-amplitude reflections where they are present.



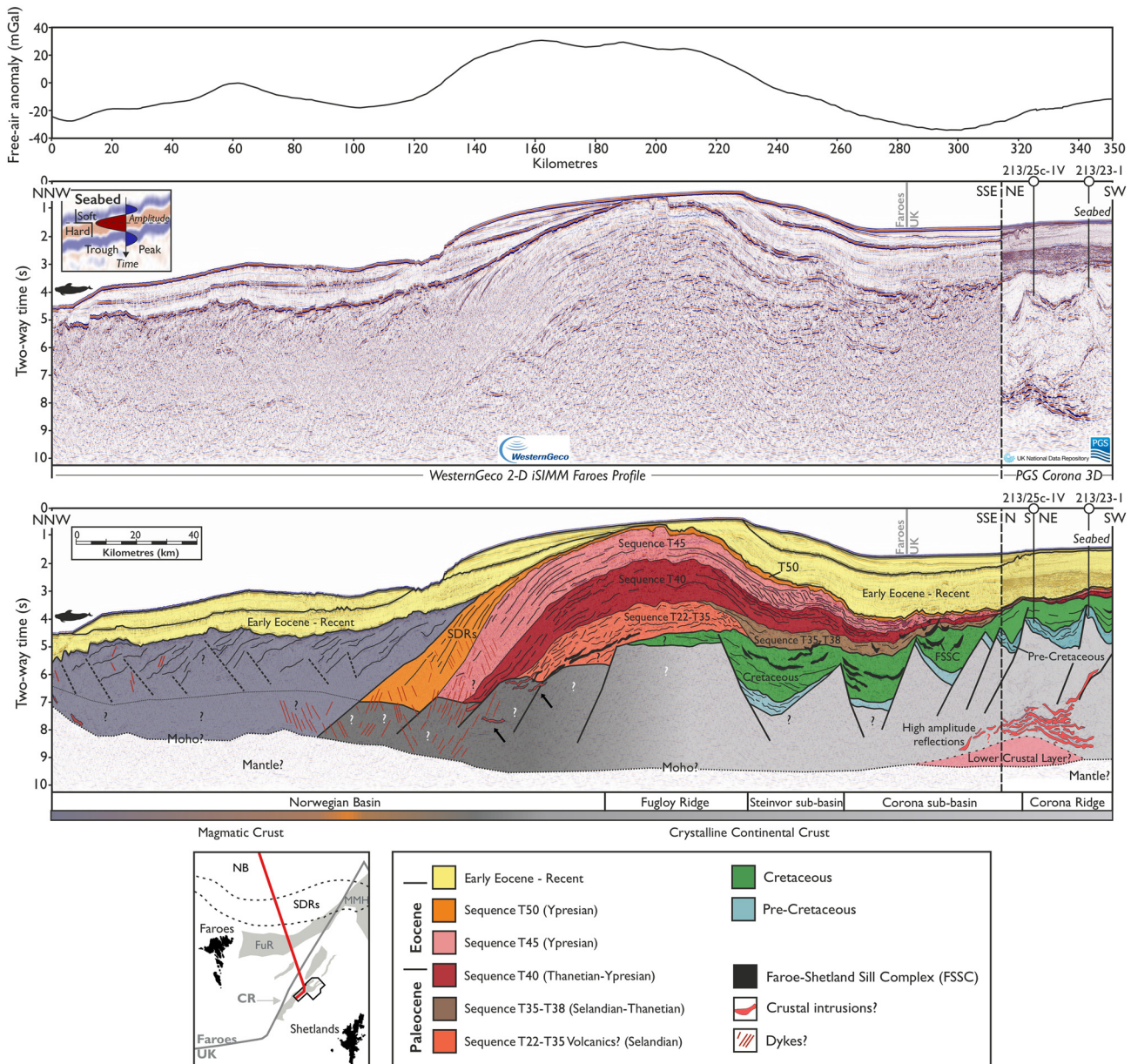


**Fig. 2.** Arbitrary regional seismic line and geoseismic interpretation across 350 km of the NE Atlantic Margin with corresponding free air gravity anomaly data shown in the upper panel. The seismic line goes through the Norwegian Basin (Faroese sector; Fig. 1), the Fugloy Ridge and into the FSB to the central-northern Corona Ridge through hydrocarbon exploration wells 213/25c-1V (North Uist) and 213/23-1 (Eriboll). The 2D iSIMM Faroes profile is used with their permission. The 3D seismic reflection data (right-hand side of panels) was acquired by PGS Exploration for Total E&P U.K. Ltd and partners between 2013 and 2015 and are freely available from the North Sea Transition Authority National Data Repository. The free air gravity anomaly data are from the International Gravimetric Bureau World Gravity Map 2012 Global Model and are publicly available. The location of the seismic line is shown in Figure 1. The lower crustal intrusions interpreted by White *et al.* (2008) and discussed in the text are the crustal intrusions at *c.* 6–7 s TWT, *c.* 160 km along the 2D iSIMM Faroes profile, highlighted by the arrow in the lower panel. CR, Corona Ridge; FuR, Fugloy Ridge; MMH, Møre Marginal High; NB, Norwegian Basin; SDRs, seaward-dipping reflections.

### Use of the term magmatic underplating

The addition of ultramafic magma at the Moho and/or the addition of mafic magma into the lower crust was termed magmatic underplating by Cox (1980, 1993). Despite Cox (1980) originally intending the term magmatic underplating to include lower crustal intrusion, many workers have interpreted magmatic underplating to only refer to the addition of magma to the base of the crust at the Moho. As a result, the use of the term magmatic underplating was reviewed by White and Smith (2009) and White *et al.* (2010), who describe its usage as ‘blurred’ (White and Smith 2009) and ‘sometimes erroneous’ (White *et al.* 2010). Therefore, to avoid any misunderstanding of the term,

we only use magmatic underplating here when discussing and citing previous work. Instead, the addition of magma within the lower crust is referred to as lower crustal intrusion. Since magmatic underplating was first suggested by Cox (1980) and developed further by White and McKenzie (1989a, b), Fyfe (1992) and Cox (1993), advances in seismic acquisition and processing have facilitated the imaging of deeper crustal structures (see Hardwick *et al.* 2010; Joseph *et al.* 2017), which have indicated the existence of crustal reflectivity interpreted as intrusions in areas located along the NE Atlantic Margin (see Mjelde *et al.* 2001; Smith *et al.* 2005; Cartwright and Hansen 2006; White *et al.* 2008, 2010; Abdelmalak *et al.* 2017; Wrona *et al.* 2019b).



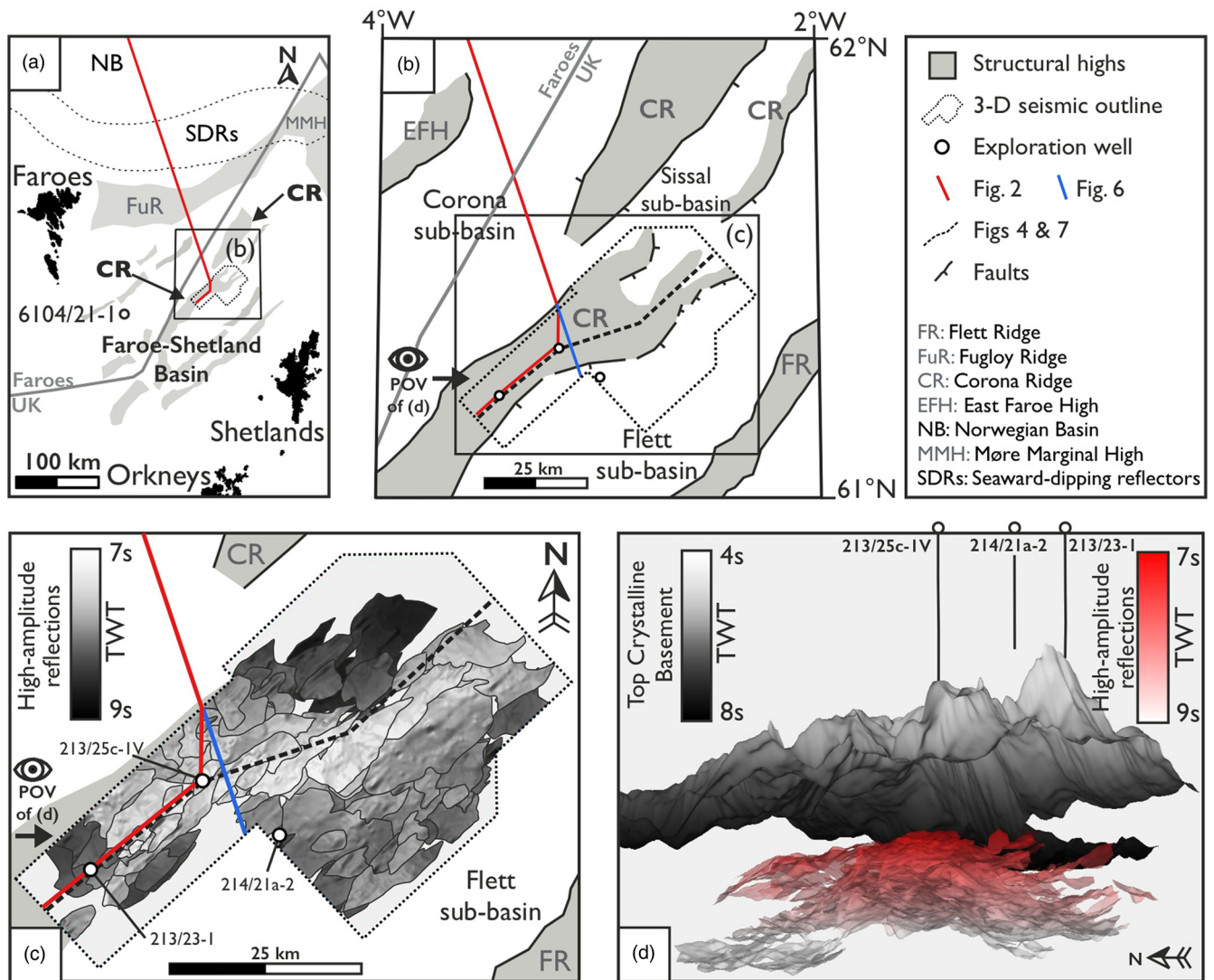


**Fig. 3.** (a) Map showing the area of the Faroe–Shetland Basin, coverage of the 3D seismic survey (dashed line), the seismic line shown in Figure 2 (red line), the key structural elements and seaward-dipping reflections from Funck *et al.* (2016), together with the location of part (b) and exploration well 6104/21-1 (Brugdan 1). (b) Map of the study area showing the coverage of the 3D seismic survey (dashed line) and the key structural elements, together with the locations of Figures 2, 4, 5 and 7, the exploration wells drilled within the seismic dataset and the point of view of part (d). (c) Time map of the lower crustal high-amplitude reflections, together with the location of exploration wells drilled within the 3D seismic reflection dataset. (d) 3D view of the lower crustal high-amplitude reflections (red scale) beneath the top-crystalline-basement surface (grey scale) mapped in this study. Point of view is from the west looking east and is shown in parts (b) and (c). Note that the lower crustal high-amplitude reflections form a dome shape. POV, point of view. Source: In part (a), the intra-basinal highs (grey shapes) are from Moy and Imber (2009), Hardman *et al.* (2018a) and the structure of the Corona Ridge within the study area is from Layfield *et al.* (2022).

### Lower crustal intrusion along the NE Atlantic Margin

The type of data used to infer the presence of lower crustal intrusions along the NE Atlantic Margin generally falls into one of three categories: (1) seismic refraction and velocity data revealing high-velocity zones or layers within the lower crust and/or at the Moho; (2) seismic reflection data revealing deep crustal reflectivity; and (3) non-seismic data (e.g. petrological, geochemical, vitrinite reflectance and apatite fission track data).

#### Seismic refraction and velocity data

Within the lower crust beneath the Faroe Islands (Richardson *et al.* 1998), Hatton Bank (Smith *et al.* 2005), Fugloy Ridge (White *et al.* 2010; Eccles *et al.* 2011) and the Vøring area (Mjelde *et al.* 2001, 2009), high-velocity layers (P-wave velocities from 7000 to >8400 m s<sup>-1</sup>; Table 1) are generally interpreted as lower crustal igneous bodies or highly intruded crust at the Moho. High-velocity

layers are also used to infer up to 15 km of magmatic underplating beneath parts of the Hatton–Rockall (White *et al.* 1987) and the Vøring areas (Hinz *et al.* 1987; Mjelde *et al.* 2001, 2009).

#### Seismic reflection data

Evidence of seismic reflectivity within the crust is documented within the Northern North Sea (McBride *et al.* 2004; Wrona *et al.* 2019b), the Norwegian Basin (Faroes sector; Fig. 1) (Smith *et al.* 2005; White *et al.* 2008, 2010) and the Vøring area (Mjelde *et al.* 2001; Gemigon *et al.* 2003, 2004; Cartwright and Hansen 2006; Abdelmalak *et al.* 2017; Kilhams *et al.* 2021), where crustal reflectivity has been interpreted to represent igneous intrusions. Mafic intrusions emplaced within the lower crust may produce strong reflectivity with reflection coefficients from  $\pm 0.10$  (Warner 1990) up to  $\pm 0.18$  (Deemer and Hurich 1994). However, McBride *et al.* (2004) suggests that the addition of magma into the lower crust does not always produce reflectivity. The nearest example of crustal

**Table 1.** Published density and velocity values for crystalline continental crust, the upper mantle, high-velocity layers at the Moho and lower crustal intrusions

Reference	Density (kg m <sup>-3</sup> )	Velocity (m s <sup>-1</sup> )
<i>Crystalline continental crust</i>		
Funck <i>et al.</i> (2014)	2750–2950	
Abdelmalak <i>et al.</i> (2017)		6000–6500
Chadwick and Pharaoh (1998)		6200–6600
Ripponington <i>et al.</i> (2015)	2790–2900	6500–7700
<i>High-velocity lower crustal layer/body</i>		
White <i>et al.</i> (2010)		6700–7300
Abdelmalak <i>et al.</i> (2017)		7000
Ernst (2014)		7000–8000
Smith <i>et al.</i> (2005)		7100–7500
White <i>et al.</i> (1987)		7300–7400
Chadwick and Pharaoh (1998)	3500	>8400
<i>Lower crustal intrusions</i>		
Maclennan and Lovell (2002)	<i>c.</i> 2800–2900	
Lyngsie and Thybo (2007)	2900–2930	7000
Richardson <i>et al.</i> (1998); White <i>et al.</i> (2008)		7000
Furlong and Fountain (1986)	3000	7000–8100
Mjelde <i>et al.</i> (2001)		7100–7800
Fernández <i>et al.</i> (2004)	3000	
Funck <i>et al.</i> (2014)	3100	
White and McKenzie (1989 <i>a, b</i> )	3300	>7200
Mjelde <i>et al.</i> (2016)	3300–3500	8000–8500
<i>Upper mantle</i>		
Maclennan and Lovell (2002)	3200	
Funck <i>et al.</i> (2014, 2016)	3200	>8000
Ripponington <i>et al.</i> (2015)	3300	8000
Brodie and White (1995)	3330	
Abdelmalak <i>et al.</i> (2017)		>8000

The values were used to inform the inputs into the velocity models (for depth conversion) in Figure 4 and the gravity models in Figure 7.

reflectivity to the FSB is NW of the Fugloy Ridge beneath the Norwegian Basin (Faroese sector; Fig. 1) along the 2D iSIMM Faroes profile (Smith *et al.* 2005; White *et al.* 2008, 2010).

#### Non-seismic data

In contrast with other areas located along the NE Atlantic Margin, where seismic evidence of lower crustal reflectivity is documented, only non-seismic data have been used to infer the presence of magmatic underplating beneath the FSB, mainly through the analysis of petrological and geochemical data that has been used to identify anomalous vertical motion (Shaw-Champion *et al.* 2006, 2008; Ritchie *et al.* 2011).

To account for subsidence anomalies, Clift and Turner (1998, p. 238, their fig. 8) interpreted underplate thicknesses of 1–5 km within the FSB, with thicknesses of *c.* 3–4 km inferred beneath the Corona Ridge area. Based on petrological and geochemical evidence, Chambers and Fitton (2000) and Maclennan and Lovell (2002) proposed that substantial quantities of magma were added to the continental crust beneath western Scotland at *c.* 60 Ma (during the Selandian). By reconstructing the palaeo-heat flow from vitrinite reflectance and apatite fission track data, Clift (1999) suggested that if magmatic underplating occurred beneath the FSB, then it took place progressively over *c.* 11 myr via the accretion of magma (see Cox 1980; White and McKenzie 1989*a, b*; Cox 1993). Based on petrological and geochemical evidence, the lower crustal intrusions have been proposed as gabbroic in composition (Brodie and White 1995; Clift 1997). Various other types of data have also been used to infer a relationship between Paleogene uplift and the possible

addition of magma within the lower crust during periods of Paleogene magmatism (Brodie and White 1994, 1995; White and Lovell 1997; Jones *et al.* 2002; Tiley *et al.* 2004; Smallwood 2008).

The addition of magma at the Moho and/or within the lower crust within a relatively short period of geological time is also thought to have exerted a significant control on permanent Paleogene uplift and the subsequent deposition of Paleocene–Eocene sequences in basins located along the NE Atlantic Margin, including the FSB (Brodie and White 1994, 1995; Nadin *et al.* 1997; White 1997; White and Lovell 1997; Clift and Turner 1998; Naylor *et al.* 1999; Jones *et al.* 2002; Maclennan and Lovell 2002; Tiley *et al.* 2004; Rudge *et al.* 2008; Smallwood 2008). However, Shaw-Champion *et al.* (2008) argued that, for Paleogene uplift to be generated by magma emplacement into the lower crust and/or at the Moho, several kilometres of magma emplacement would be required, while also highlighting the lack of direct evidence for lower crustal intrusion within the study area at the time of publication.

#### Data used to identify and constrain lower crustal reflectivity

The seismic reflection dataset used in this study (see Figs 2–6) is a broadband 3D seismic survey acquired using GeoStreamer® PGS technology (see Hardman *et al.* 2018*b*). The Galloway/Corona 3D seismic survey covers an area of *c.* 1850 km<sup>2</sup> (*c.* 37 km × 68 km, Figs 1, 2) and the data extend down to *c.* 10 s TWT (*c.* 25 km depth). The seismic reflection data were acquired by PGS Exploration for hydrocarbon exploration by Total E&P U.K. Ltd and partners in two phases: phase-1 in 2013 (Galloway) and phase-2 in 2015 (Corona); the key acquisition parameters of each phase are summarized in Table 2. The use of GeoStreamer® PGS technology facilitated recording of the low frequencies (<10 Hz) crucial in imaging deeper crustal structures, which, alongside Kirchhoff prestack time migration, resulted in a broader bandwidth, amplitude preservation and substantial improvements in the signal-to-noise ratio, producing a significant uplift in image quality compared with vintage 3D reflection data (see Joseph *et al.* 2017). For detailed information on the processing of the 3D dataset, see PGS Imaging (2016).

At near-top Cretaceous levels, at *c.* 3.5 s TWT (*c.* 3 km depth, Fig. 4), the dominant frequency of the seismic data is *c.* 22 Hz, giving a vertical resolution (*c.*  $\lambda/4$ ) of *c.* 31 m (assuming a Cretaceous velocity of 2720 m s<sup>-1</sup>, see Fig. 4 and Table 3). At deeper base Cretaceous levels, at *c.* 6.5 s TWT (*c.* 10 km depth, Fig. 4), the dominant frequency of the seismic reflection data decreases to *c.* 8 Hz, giving a vertical resolution (*c.*  $\lambda/4$ ) of *c.* 85 m. These estimates use interval velocities obtained from hydrocarbon wells drilled within the 3D seismic reflection dataset (213/23-1, 213/25c-1V and 214/21a-2; see Table 3). Between *c.* 7 and 9 s TWT (the typical depths at which high-amplitude reflections were mapped in this study), the dominant frequency decreases to between 5 and 8.5 Hz, giving vertical seismic resolutions (*c.*  $\lambda/4$ ) between 191 and 325 m, assuming a velocity of 6500 m s<sup>-1</sup> for the crystalline continental crust (Chadwick and Pharaoh 1998; Ripponington *et al.* 2015; Abdelmalak *et al.* 2017; see Table 1). Detectability (*c.*  $\lambda/8$ ) between 7 and 9 s TWT is therefore estimated to be between *c.* 96 and *c.* 163 m. The detectability and resolution of the seismic data used in this study dictate our ability to identify igneous intrusions of varying thickness and to ultimately calculate emplaced magma volumes and the potential Paleogene uplift that may be associated with intrusion emplacement.

Other seismic data used within this study include the multiclient 2D iSIMM Faroes profile (315 km are shown in Fig. 2), which was acquired by WesternGeco in 2002 as part of the Integrated Seismic Imaging & Modelling of Margins (iSIMM) project led by academics and petroleum industry partners. The 2D iSIMM Faroes profile is used to provide the regional context and,



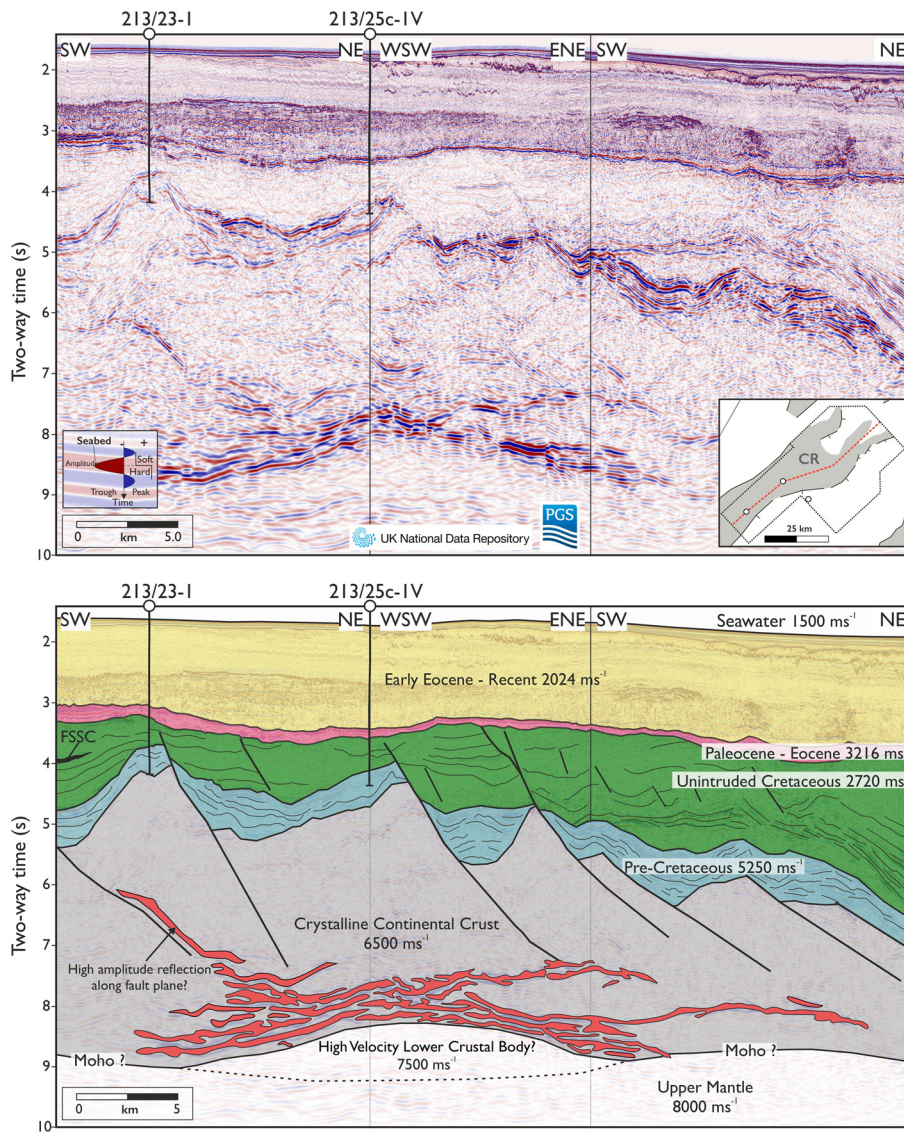


**Fig. 4.** NE–SW arbitrary seismic line and geoseismic interpretation along the central-northern Corona Ridge through exploration wells 213/23-1 (Eriboll) and 213/25c-1V (North Uist). The model shows the interval velocities used to depth-convert the seismic line shown for gravity modelling (Fig. 4). The velocities of the crystalline basement ( $6500 \text{ m s}^{-1}$ ), gabbroic lower crustal layer ( $7500 \text{ m s}^{-1}$ ) and mantle ( $8000 \text{ m s}^{-1}$ ) were assigned based on the velocities recorded from seismic refraction surveys within the Faroe–Shetland Basin (Table 1). The average interval velocities of sedimentary sections were obtained from exploration wells drilled within the 3D seismic reflection dataset (213/23-1, 213/25c-1V and 214/21a-2); the values for each interval within each well are given in Table 3. For gravity models C (Fig. 7c) and D (Fig. 7d), the velocity model used to convert the seismic line from time to depth was the same; however, a high-velocity lower crustal layer with a velocity of  $7500 \text{ m s}^{-1}$  (dashed line) at the base of the crust (the Moho) was included. The 3D seismic reflection data were acquired by PGS Exploration for Total E&P U.K. Ltd and partners and are available from the North Sea Transition Authority National Data Repository. Note: high-amplitude reflections are shown in red and the Faroe–Shetland Sill Complex is shown in black. CR, Corona Ridge.

specifically, to enable comparison between the lower crustal reflections beneath the Corona Ridge and the most proximal interpretation of lower crustal intrusions described by Smith *et al.* (2005) and White *et al.* (2008, 2010) beneath the Norwegian Basin (Farøese sector; Fig. 1). The 2D iSIMM Farøes profile was acquired by WesternGeco's Topaz acquisition vessel using coincident wide-angle OBS acquisition and long-offset multi-Q-streamer (two streamers, each 12 km in length) 2D swaths and arguably represented the most advanced imaging at the time (White *et al.* 2002, 2010). 2D seismic data, which are not shown here, but are publicly available from Jarðfeingi (the Farøese Geological Survey), extend through the nearest offset wells to drill through thick volcanic sequences on the East Farøe High (Fig. 1b) and were used to extrapolate volcanic sequences *c.* 100 km from wells 6104/21-1 (Brugdan 1) and 6104/21-2 (Brugdan 2) (see Jolley *et al.* 2021, p. 72, their fig. 9) through the series of 2D lines to aid the interpretation of the 2D iSIMM Farøes profile (Fig. 2). The 3D seismic reflection data and 2D iSIMM Farøes profile are displayed at zero-phase negative standard European polarity (Sheriff and Geldart 1982). A downward increase in acoustic impedance (hard) is associated with a negative amplitude (trough) shown in red and a downward decrease in acoustic impedance (soft) is associated with a positive amplitude (peak) shown in blue.

The free air gravity anomaly data (Fig. 1b) are from the International Gravimetric Bureau (BGI) World Gravity Map 2012

Global Model and were used to perform gravity modelling (Fig. 7). These gravity data are publicly available from the BGI and are described in detail by Balmino *et al.* (2011). The geothermal well data shown in Figure 8 are predominantly from the CGG Geothermal Database, which is freely available from the North Sea Transition Authority (NSTA) Open Data site. Geothermal data for wells located along the Corona Ridge are not included within the CGG database and were obtained from corrected bottom hole temperature values within each end of well report, which are freely available from the NSTA National Data Repository. The geothermal gradients given within Figure 8 are an average over the entire depth of the well. Other well data used for the purpose of this study were also downloaded from the NSTA National Data Repository (NSTA 2022), where they are freely available.

## Methods

### Seismic interpretation

All of the high-amplitude reflections towards the base of the crust interpreted in this study are either at or below the vertical resolution (*c.*  $\lambda/4$ , 191–325 m) of the 3D seismic reflection data at depths of 7–9 s TWT and are therefore tuned and detected as only one reflection. In general, according to Sheriff and Geldart (1982), reflections thinner than *c.*  $\lambda/8$  (96–163 m) are not detected. However,



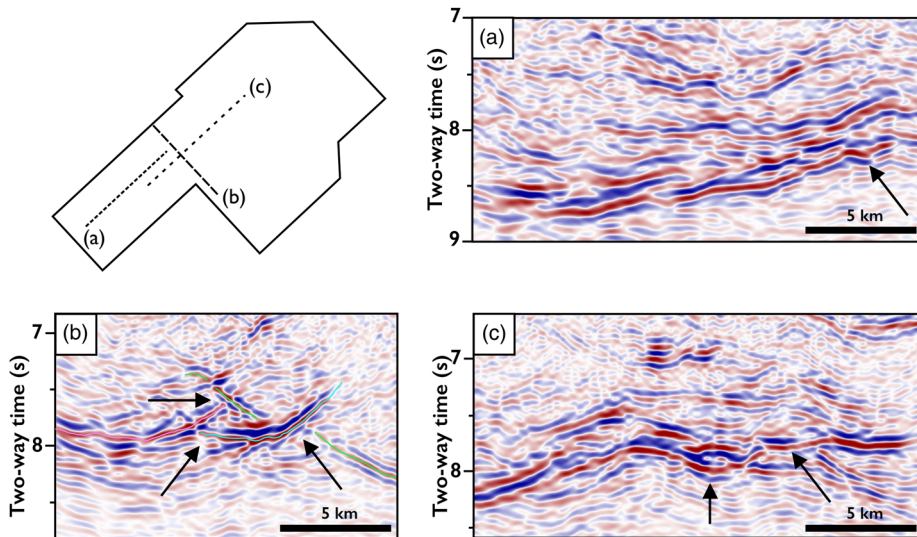


**Fig. 5.** Seismic lines showing examples of the high-amplitude reflections in detail. The location of each seismic line is shown on the outline of the 3D seismic data in the top-left panel. (a) The arrow points to an example of a wing-like geometry at the edge of a high-amplitude reflection. (b) An example of how some of the high-amplitude reflections have cross-cutting and intersecting relationships with other high-amplitude reflections. The arrows highlight where the high-amplitude reflections intersect other high-amplitude reflections. (c) The arrow on the left shows the bowl-like shape of one high-amplitude reflection that also has a wing geometry (the arrow on the right) originating from the bowl-like area of the reflection.

depending on the signal-to-noise ratio of the seismic data, detectability may be closer to  $c. \lambda/32$  (Smallwood and Maresh 2002). Within the 3D seismic data at the depths at which the high-amplitude reflections are imaged ( $c. 7-9$  s TWT), detectability may therefore be as low as 24–41 m ( $\lambda/32$ ). Ultimately, calculating the thicknesses of seismic reflections that will never be penetrated by a hydrocarbon well will always be challenging and will always produce large uncertainties. Acknowledging this, the thicknesses of the high-amplitude reflections were calculated using  $\lambda/32$ ,  $\lambda/8$  and  $\lambda/4$  (Table 4) to provide a range of potential thickness and volume estimates for the high-amplitude reflections.

Mapped reflections were identified based on their high amplitude. The high-amplitude reflections were interpreted using manual picking and were then interpolated to create continuous 3D

surfaces. The area of the 3D surface (high-amplitude reflection) was then multiplied by the vertical resolution ( $c. \lambda/4$ ) and also the potential limits of detection ( $c. \lambda/8$  and  $\lambda/32$ ) of the seismic data at the depth of the reflection (used as an indicator of reflection thickness as the reflections are tuned; see Mark *et al.* 2018a) to obtain a range for the estimate of the volume of the reflections.

If the high-amplitude reflections represent lower crustal intrusions, then there are likely to be substantially more intrusions present than are resolved (Schofield *et al.* 2017). Based on well penetrations of sedimentary sections within the FSB, Mark *et al.* (2018a) showed that, for a given 50 m thick igneous intrusion, there may be an extra  $c. 70$  m of disseminated igneous material that is too thin to be resolved in seismic data (a ratio of 1:1.4 m for resolved to unresolved igneous material; Mark *et al.* 2018a). The work of Mark

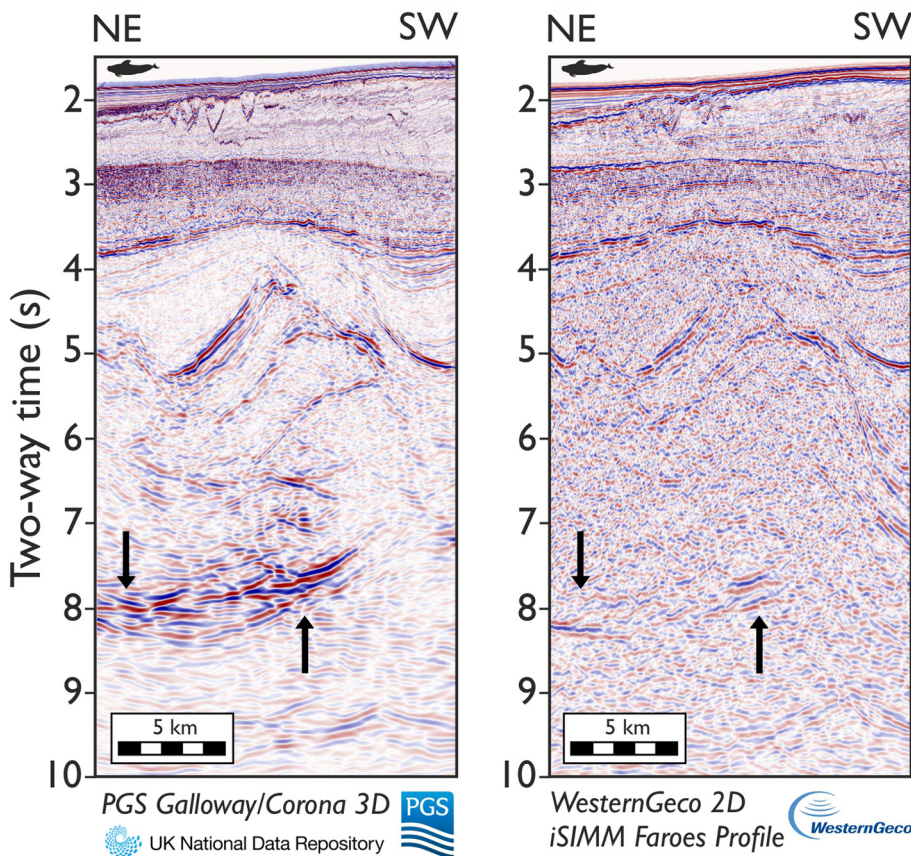


**Fig. 6.** NE-SW seismic lines through the same section of the central-northern Corona Ridge within both the PGS Galloway/Corona 3D (left panel) and 2D iSIMM Faroes profile (right panel) showing the presence of the high-amplitude reflections between 7 and 9 s TWT within both datasets (highlighted by the arrows), which were processed separately. The 3D seismic reflection data (left panel) were acquired by PGS Exploration for Total E&P U.K. Ltd and partners in 2013 and 2015 and are available from the North Sea Transition Authority National Data Repository. The 2D iSIMM Faroes profile (right panel) was acquired by WesternGeco in 2002 and is shown with their permission. For the location of both lines, see Figure 3b (blue line).



**Table 2.** Key parameters of the phase 1 and phase 2 acquisition of the Galloway/Corona 3D seismic survey used in this study from Layfield *et al.* (2022)

Acquisition parameter	Phase 1: Galloway 2013	Phase 2: Corona 2015
Dual source depth (m)	9	9
No. of streamers	12	10
Streamer towing depth (m)	20	20
Streamer spacing (m)	100	100
Streamer cable length (m)	6000	7050
Near-trace offset (m)	200	99
Shot interval (m)	25	25

*et al.* (2018a) is concerned with estimating the amount of unresolved seismic material within sedimentary sequences based on seismic and well data within the FSB. To date, no work has focused on the relative proportions of resolved to unresolved intrusions within continental crystalline crust. We use the ratio of 1:1.4 m to provide an estimate of the amount of unresolved material that may be associated with the high-amplitude reflections. The obvious caveat of this method is that it assumes the proportions and distributions of resolved and unresolved igneous intrusions within the lower crust and within sedimentary basins are comparable.

The term cumulative thickness refers to the total thickness of lower crustal reflections stacked on top of one another at one location within the study area or within a 2D seismic line from the 3D seismic reflection data. Where the term total volume is used, this refers to the sum of all the volumes calculated for all individual reflections mapped throughout the entire 3D dataset.

### Gravity modelling

To test our seismic interpretation, the gravity responses for four different geological interpretations (four scenarios; Fig. 7) were modelled. Gravity modelling was conducted along a single 2D line (Fig. 4) across the central-northern Corona Ridge through hydrocarbon wells 213/23-1 (Eriboll) and 213/25c-1V (North Uist) using the ARK CLS XField plug-in for Schlumberger Petrel software. By combining the average density (obtained from the bulk density logs of hydrocarbon exploration wells 213/23-1, 213/25c-1V and 214/21a-2, Table 5) and the thickness of each specified interval (based on the depth-converted interpreted surfaces; Figs 4, 6), the ARK CLS XField Petrel plug-in computes the theoretical gravity signature above the location of the 2D line, located along the central-northern Corona Ridge (Fig. 4). We use the term ‘interval’ here to mean, for example, the Cretaceous interval (intervals are delineated by horizons; see Fig. 4). The modelled gravity signature of the four different geological interpretations were then compared with the observed free air gravity anomaly from the BGI World Gravity Map 2012 Global Model. Gravity modelling is limited to 2D and is limited in resolution (i.e. not all heterogeneities in rock

densities can be captured within each model). To reduce edge effects, the model was assumed to extend laterally to infinity.

### Depth conversion

To create the 2D gravity models, depth conversion of a seismic line (Fig. 4, location shown in Fig. 1) from the Galloway/Corona 3D seismic reflection data using the average velocities between each of the interpreted horizons (Fig. 4 and Table 3) was undertaken. These velocities (Fig. 4 and Table 3) were obtained from the average interval velocities of sedimentary sections penetrated by wells drilled within the 3D seismic dataset (wells 213/23-1, 213/25c-1V and 214/21a-2; Fig. 3). The Cretaceous interval velocity ( $2720 \text{ m s}^{-1}$ ) is relatively low compared with other published values throughout the FSB (see Rippington *et al.* 2015; Walker *et al.* 2021), which is possibly a result of differential compaction over the Corona Ridge structural high compared with the basinal areas and a lack of igneous intrusion emplacement along the central-northern Corona Ridge within the Cretaceous strata (Fig. 4; see also Layfield *et al.* 2022). The velocities of the crystalline basement ( $6500 \text{ m s}^{-1}$ ), gabbroic lower crustal intrusions ( $7200 \text{ m s}^{-1}$ ), gabbroic lower crustal layer ( $7500 \text{ m s}^{-1}$ ) and the mantle–upper mantle ( $8000 \text{ m s}^{-1}$ ) were assigned based on previously published values throughout the FSB (Chadwick and Pharaoh 1998; White *et al.* 2008; Rippington *et al.* 2015), the Faroe Islands (Richardson *et al.* 1998) and other areas located along the NE Atlantic Margin (White *et al.* 1987, 2008; Mjelde *et al.* 2001, 2016; Smith *et al.* 2005; Ernst 2014; Abdelmalak *et al.* 2017). The ranges of these published velocities are shown in Table 1. As a result of using single values assigned from the published range shown in Table 1, there will be increased potential errors in the depth conversion at depth compared with shallower regions in the depth-converted seismic sections, where the interval velocities were obtained from data obtained within hydrocarbon wells.

### Rock densities

The average densities of each interval (Fig. 7 and Table 5) were calculated from the bulk density logs of hydrocarbon exploration wells within the study area (wells 213/23-1, 213/25c-1V and 214/21a-2) using Schlumberger’s Techlog software. Densities of the crystalline basement ( $2750 \text{ kg m}^{-3}$ ), gabbroic lower crustal intrusions ( $3100 \text{ kg m}^{-3}$ ) and the upper mantle ( $3300 \text{ kg m}^{-3}$ ) were assigned based on a range of published values throughout the NE Atlantic Margin (Table 1). Along the NE Atlantic Margin, lower crustal intrusions are thought to be gabbroic in composition (Brodie and White 1995; Clift 1997). We assigned a density of  $3200 \text{ kg m}^{-3}$  to the lower crustal layer within the gravity models in Fig. 6c, d. Although a density of  $3200 \text{ kg m}^{-3}$  is lower than that proposed by Chadwick and Pharaoh (1998) of  $3500 \text{ kg m}^{-3}$  (see Table 1), a lower crustal layer must be less dense than the upper mantle ( $3300 \text{ kg m}^{-3}$ ), but denser than the crystalline continental crust ( $2750 \text{ kg m}^{-3}$ ), to be emplaced at the Moho (Cox 1980, 1993; White and McKenzie 1989a, b).

**Table 3.** Average interval velocities of key stratigraphic units used for depth conversion

Well No.	Average interval velocity ( $\text{m s}^{-1}$ )			
	Early Eocene–Recent	Paleocene–Eocene	Cretaceous	Pre-Cretaceous
213/23-1	1961	3190	2698	5112
213/25c-1V	1972	3578	2742	5387
214/21a-2	2140	2880		
Average	2024	3216	2720	5250

Interval velocities calculated from exploration wells (listed in first column) drilled within the 3D seismic reflection dataset.

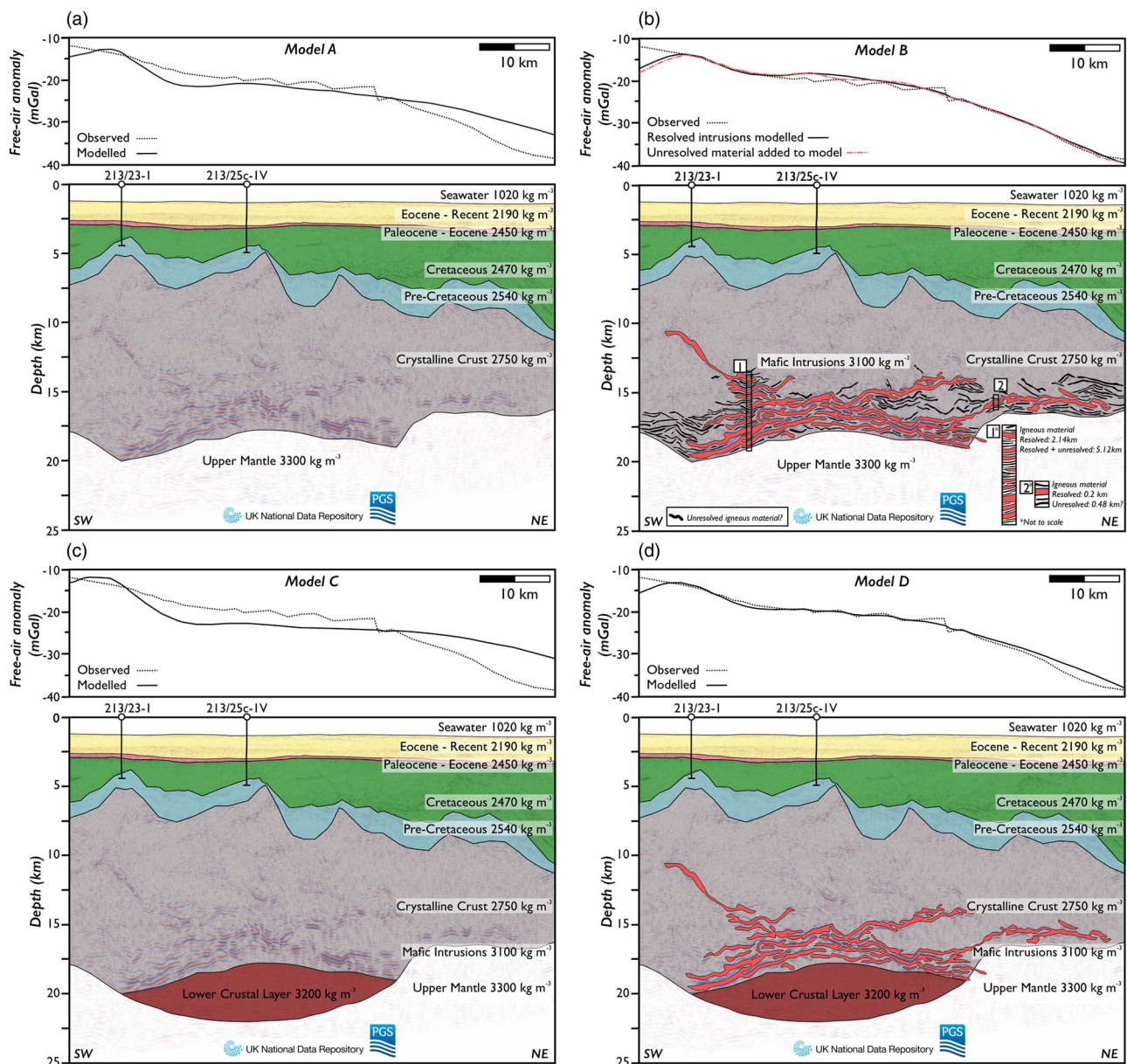


**Fig. 7.** Modelled gravity responses of four interpretations along the central-northern Corona Ridge (Faroe–Shetland Basin) with the observed free air gravity anomaly. The location of the depth-converted seismic line is shown in [Figure 1](#) (also shown in time in [Fig. 4](#)). The densities used as input to the gravity model (see [Table 5](#)) are shown on the depth-converted seismic line and were obtained from hydrocarbon exploration wells drilled within the 3D seismic reflection dataset (213/23-1, 213/25c-1V and 214/21a-2). The densities of the crystalline basement ( $2750 \text{ kg m}^{-3}$ ), gabbroic lower crustal layer ( $3200 \text{ kg m}^{-3}$ ), lower crustal intrusions ( $3100 \text{ kg m}^{-3}$ ) and the mantle ( $3300 \text{ kg m}^{-3}$ ) were assigned based on published values along the NE Atlantic Margin (see [Table 1](#)). (a) Model A: no igneous intrusion modelled within the lower crust. (b) Model B, which consists of two sub-models. Sub-model 1 models the high-amplitude reflections mapped as part of this study (overlain in red) as igneous intrusions within the lower crust (see [Figs 3, 4](#)), with the modelled gravity response shown by the solid black line. The second sub-model consists of both the resolved reflections mapped by this study (overlain in red) and the potentially unresolved disseminated lower crustal intrusions (overlain in black), with the modelled gravity response shown by the dashed red line. We cannot accurately distribute the unresolved material throughout the gravity model; this material is modelled purely to show the response of adding potentially unresolved extra igneous material. (c) Model C: no igneous intrusion modelled within the lower crust, but a lower crustal layer is modelled at the Moho. (d) Model D: igneous intrusions (high-amplitude reflections) within the lower crust (as shown in [Fig. 1](#)) and a lower crustal layer modelled at the Moho (models B and C combined). Note that different geometries of the lower crustal intrusions and the Moho (the base of the crystalline basement) between [Figures 4](#) and [6](#) is due to time–depth conversion. The 3D seismic reflection data were acquired by PGS Exploration for Total E&P U.K. Ltd and partners and are available from the North Sea Transition Authority National Data Repository. No structural interpretation is added to the figure as this was not modelled.

### Estimating uplift

Thickness estimates for the lower crustal reflections (including unresolved igneous material) were used to estimate the uplift that may be associated with the potential emplacement of lower crustal intrusions. The isostatic equation (1) used to estimate uplift is based on work by [Brodie and White \(1994, 1995\)](#) (see also [Allen and Allen 2013](#)). This equation facilitates the thickness and densities of

the lower crustal intrusions (magmatic underplate) and mantle to be considered within the calculation.

$$U = T_{\text{LCIs}} \times \left[ 1 - \left( \frac{\rho_{\text{LCIs}}}{\rho_{\text{mantle}}} \right) \right]$$

where  $\rho_{\text{mantle}}$  is the density of the mantle (here,  $3300 \text{ kg m}^{-3}$ ),  $\rho_{\text{LCIs}}$  is the density of lower crustal intrusions (here,  $3100 \text{ kg m}^{-3}$ ),  $T_{\text{LCIs}}$



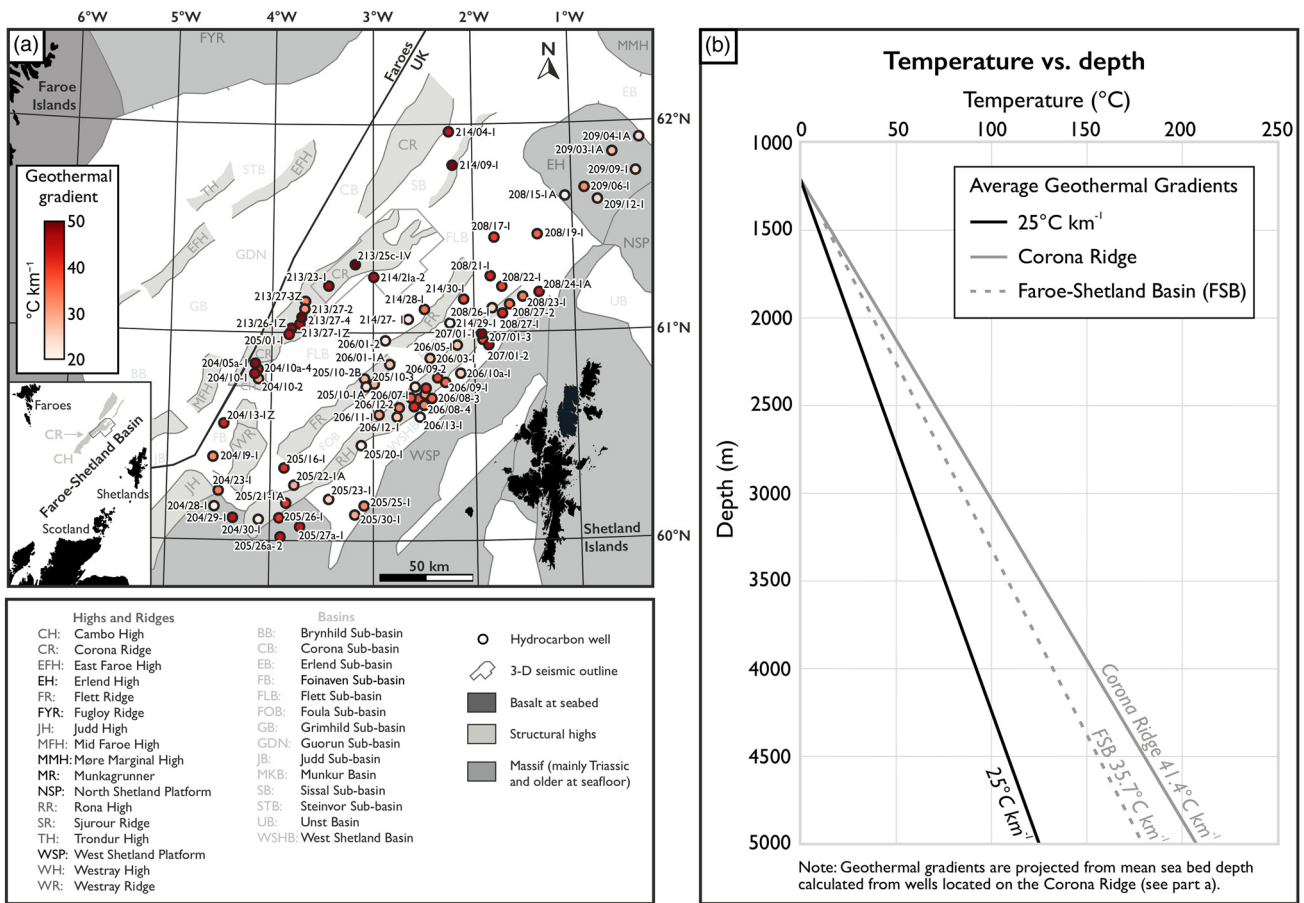


**Fig. 8.** (a) Map of the Faroe–Shetland Basin showing the key structural elements and coverage of the Galloway/Corona 3D seismic survey. The map is overlain with the wells located within the Faroe–Shetland Basin where geothermal data were available from the CGG Geothermal Database (freely available from the North Sea Transition Authority Open Data site). Geothermal gradients of the wells located along the Corona Ridge (in Quadrants 213 and 214) were calculated using wells from the North Sea Transition Authority National Data Repository and are not freely available as part of the CGG Geothermal Database. Note the darker colours (higher geothermal gradients) located along the Corona Ridge compared with wells throughout the rest of the basin. (b) Graph showing the average temperature v. depth relationships (geothermal gradients) for the Faroe–Shetland Basin (dashed grey line), the Corona Ridge (solid grey line) and a geothermal gradient of 25°C km<sup>-1</sup> (solid black line) typical of continental crustal domains located along passive margins (Allen and Allen 2013). The graph shows that the average geothermal gradient (41.4°C km<sup>-1</sup>) calculated for the wells located along the Corona Ridge (see Fig. 8a) is 5.7°C km<sup>-1</sup> higher than the average geothermal gradient of the Faroe–Shetland Basin (35.8°C km<sup>-1</sup>). Note: (1) the geothermal gradients are projected from mean seabed depth calculated from wells located along the Corona Ridge (see Fig. 8a), where the average temperature is c. 1°C, allowing the geothermal gradients to be compared and (2), where the well density is high (e.g. in Quadrant 206), the wells may not be in the exact location drilled because they have been moved slightly to allow the colour fill of the well to be observed and therefore not all the wells have been labelled. Sources: part (a) location of the structural elements modified from Ritchie *et al.* (2011), figure 7 and Mark *et al.* (2018b) with intra-basinal highs modified from Ellis *et al.* (2009) and Hardman *et al.* (2018a) and the Corona Ridge structure within the study area from Layfield *et al.* (2022).

is the maximum thickness of the lower crustal intrusions (here, 5.12 km) and *U* is the uplift (units: km). The inputs into equation (1) for the densities of the lower crustal intrusions ( $\rho_{LCIs}$ ) and mantle ( $\rho_{mantle}$ ) are consistent with the densities used within 2D gravity modelling (Fig. 7) and those published throughout the NE Atlantic Margin (see Table 1).

**Results**

**High-amplitude reflections beneath the central-northern Corona Ridge**

We generally interpret the Moho (lower crustal boundary) (Fig. 4) to be located between c. 18 and 20 km (c. 9–10 s TWT; Figs 2–4) by

**Table 4.** Thicknesses calculated for individual lower crustal high-amplitude reflections throughout the 3D seismic reflection dataset

	Mapped reflections			Mapped plus unresolved reflections (ratio 1:1.4)		
	$\lambda/32$ (min.)	$\lambda/8$	$\lambda/4$	$\lambda/32$	$\lambda/8$	$\lambda/4$ (max.)
Individual reflections (m)	24–41	96–163	191–325	41–98	230–391	458–780
Maximum thickness in data (km)	0.27	1.07	2.14	0.65	2.57	5.12
Total volume in data (km <sup>3</sup> )	111	444	888	266	1065	2131

The maximum thickness within the data refers to the maximum cumulative thickness of ‘stacked’ high-amplitude reflections throughout the 3D dataset using thicknesses obtained based on  $\lambda/32$ ,  $\lambda/8$  and  $\lambda/4$ . The total volume refers to the total estimated volume of the high-amplitude reflections based on  $\lambda/32$ ,  $\lambda/8$  and  $\lambda/4$ . The right-hand side of the table shows the potential thickness and volume estimates assuming a ratio of 1:1.4 m of resolved to unresolved material. Unresolved material is assumed to be disseminated intrusions that are not imaged within the seismic data (see Mark *et al.* 2018b).

**Table 5.** Average interval densities of key stratigraphic units used for gravity models in Figure 7

Well No.	Average interval density (kg m <sup>-3</sup> )			
	Eocene–Recent	Paleocene–Eocene	Cretaceous	Pre-Cretaceous
213/23-1	2120	2460	2420	2520
213/25c-1V	2220	2420	2470	2550
214/21a-2	2240	2480	2520	
Average	2190	2450	2470	2540

Interval densities calculated from exploration wells (listed in first column) drilled within the 3D seismic reflection dataset. Bulk density correction was applied. Note: the pre-Cretaceous interval was not penetrated by hydrocarbon well 214/21a-2.

considering both a change in seismic character (e.g. impedance contrast) at these depths and work by Warner (1987). The high-amplitude reflections are mapped at depths between 14 and 20 km (c. 7–9 s TWT) and are mapped down to the Moho (c. 20 km depth).

The high-amplitude reflections appear to have a high-impedance reflectivity (a downward increase in acoustic impedance that corresponds to a negative amplitude displayed in red), although phase rotation can be an issue at such depths due to a loss of wave energy (Sheriff and Geldart 1982). In total, 131 high-amplitude reflections are mapped, with areas ranging from 1 to 200 km<sup>2</sup>. Overall, the high-amplitude reflections have an aerial extent of c. 1400 km<sup>2</sup> (comparable with the area of Greater London, 1569 km<sup>2</sup>; Greater London Authority 2018) within the 1850 km<sup>2</sup> area covered by the 3D seismic reflection dataset. Individual high-amplitude reflections have variable geometries (Fig. 5), ranging from mostly bowl-shaped (see Fig. 5c) or inclined, occasionally with tips (see Fig. 5a). The high-amplitude reflections intersect and cross-cut with other high-amplitude reflections (Fig. 5b) and most of the reflections have a tuned response.

In general, the reflections do not appear to have any relationship with the basement-bounding faults that we interpret along the central-northern Corona Ridge, except for one high-amplitude reflection (see Fig. 4) that appears to be located along a fault, but that does not reach the overlying sedimentary section above the ridge. The high-amplitude reflections appear shallower in depth (c. 14 km/7 s TWT) in the centre of the seismic reflection dataset, whereas the reflections appear deeper (c. 20 km/9 s depth TWT) towards the edges of the dataset (and the edges of the Corona Ridge). This results in an elongated, convex dome-like feature comprised of the high-amplitude reflections beneath the central-northern Corona Ridge (Fig. 3d). The high-amplitude reflections described in this study are imaged within both the 3D Galloway/Corona seismic data and within the 2D iSIMM Faroes profile at the same location (Fig. 6) and have comparable geometries. Differences between the two datasets shown in Figure 6 are therefore most likely down to different acquisition parameters and processing techniques.

Using long-offset seismic data, Makris *et al.* (2009) created a 3D model of the 7800 m s<sup>-1</sup> velocity interface over the same study area (Makris *et al.* 2009, p. 41, their fig. 13). The 3D model of the 7800 m s<sup>-1</sup> interface by Makris *et al.* (2009) similarly described an elongated dome-like structure with depths ranging between c. 14 and 18 km. This suggests that the elongated dome-like shape of the reflections we have mapped (and described here) is not unique to the 3D Galloway/Corona seismic reflection dataset used in this study (i.e. this is not a seismic artefact). The presence of the high-amplitude reflections within both the 3D Galloway/Corona seismic reflection dataset and the 2D iSIMM Faroes profile used in this study (Fig. 6), which were processed separately, also supports the notion that the high-amplitude lower crustal reflections are real features and not a seismic artefact.

Thickness estimates of individual reflections range from 24 to 326 m. Thicker accumulations of the high-amplitude reflections occur within the centre of the dataset (e.g. up to 2.14 km based on  $\lambda/4$ ;

Table 4), directly below the central-northern Corona Ridge intra-basinal high where the thickness of the crystalline continental crust is c. 12–15 km (Fig. 7; see also Badley Geoscience Limited 2019) and the sedimentary sequences are c. 5 km thick. This contrasts with the edges of the dataset, where, for example, cumulative stacked thicknesses are mostly low because only minimal high-amplitude reflections are observed and subsequently mapped (see the far NE section of Fig. 4). The maximum cumulative stacked thickness of the lower crustal reflections, which ranges from 0.27 to 2.14 km (Table 4), therefore varies markedly over short (c. 15 km) distances (Figs 4, 6). We estimate that the total volume of the high-amplitude reflections present within the 3D dataset is between 111 km<sup>3</sup> (thickness based on the lowest potential seismic detectability, c.  $\lambda/32$ ) and 888 km<sup>3</sup> (seismic resolution, c.  $\lambda/4$ ). For the full range of thickness and volume estimates based on seismic detectability ( $\lambda/32$  to  $\lambda/8$ ) and seismic resolution ( $\lambda/4$ ), see Table 4.

If the high-amplitude reflections do represent lower crustal intrusions, the estimates presented in Table 4 are likely to represent an underestimation of the amount of igneous material that may be present due to the low vertical resolutions (e.g.  $\lambda/4$ , 191–325 m) and detectability (c.  $\lambda/32$ , 101–165 m) generally encountered at the depths the high-amplitude reflections are imaged (c. 14–20 km, 7–9 s TWT), which inhibits the imaging of thinner disseminated igneous intrusions that could also be present within the lower crust. Hence, when accounting for the possible presence of unresolved material (using a 1:1.4 m ratio of resolved to unresolved intrusions), we estimate the cumulative thicknesses of the high-amplitude reflections to be between 0.65 and 5.12 km and estimate the total volumes of the reflections as between 266 and 2131 km<sup>3</sup> (Table 4).

#### Reflection coefficient: the reflectivity of lower crustal intrusions

A strong reflection (like those described here) is generally considered to have a reflectivity coefficient of c.  $\pm 0.2$  (McQuillin *et al.* 1979; Sheriff and Geldart 1982). Earlier work focused on the reflection characteristics of layered basic igneous intrusions by Warner (1990) and Deemer and Hurich (1994) suggests that cumulates intruded into the lower crust generate reflectivity (reflectivity coefficient values) of between  $\pm 0.10$  and  $\pm 0.18$ , depending on the mineralogy of the igneous material. Using the range of published values for both the density ( $\rho_1$  and  $\rho_2$ ) and velocity ( $V_1$  and  $V_2$ ) inputs of the reflectivity coefficient equation for lower crustal intrusions (2800–3500 kg m<sup>-3</sup> and 7000–8500 m s<sup>-1</sup>) and the continental crystalline crust (2750–2950 kg m<sup>-3</sup> and 6000–7700 m s<sup>-1</sup>) shown in Table 1, we tested whether a reflectivity coefficient between  $\pm 0.10$  and  $\pm 0.18$  could be theoretically obtained (Fig. 9b).

Phase rotation may occur at the deep depths (c. 14–20 km) at which the high-amplitude reflections are resolved. As the generated reflectivity coefficient range of values will be the same whether layer 1 ( $\rho_1$  and  $V_1$ ; i.e. the top layer) is a lower crustal intrusion or the



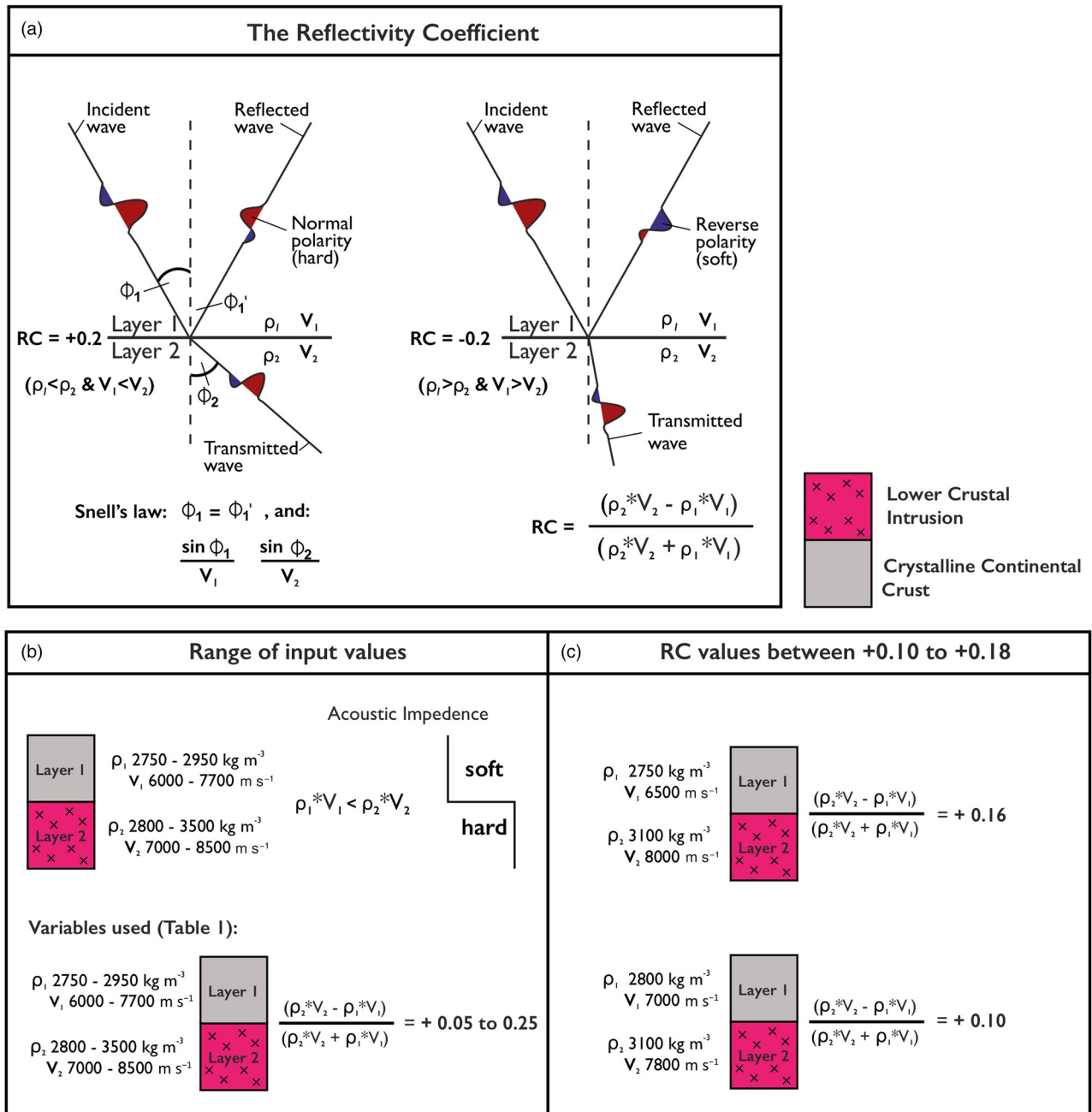


**Fig. 9.** Diagram summarizing the range of possible inputs ( $\rho_1$ ,  $\rho_2$ ,  $V_1$  and  $V_2$ ) into the reflectivity coefficient equation if the strong reflections are lower crustal intrusions emplaced within crystalline continental crust. The range of values used as inputs are based on published values across the NE Atlantic Margin (see Table 1). The ranges of the published values for the density ( $\rho_1$ ,  $\rho_2$ ) and velocity ( $V_1$ ,  $V_2$ ) of the lower crustal intrusions are 2800–3500 kg m<sup>-3</sup> and 6000–7700 m s<sup>-1</sup>, respectively, and the values for the continental crystalline crust are 2750–2950 kg m<sup>-3</sup> and 7000–8500 m s<sup>-1</sup>, respectively (see Table 1). A strong reflection is generally considered to have a reflectivity coefficient of  $c. \pm 0.2$  (McQuillan *et al.* 1979), equivalent to the reflectivity coefficient generated by a sand–shale interface (McQuillan *et al.* 1979; Sheriff and Geldart 1982). Work focused on the reflection characteristics of layered basic igneous intrusions by Warner (1990) and Deemer and Hurich (1994) suggests that cumulates intruded into the lower crust may generate reflectivity coefficients between  $\pm 0.10$  and 0.18. (a) Diagram showing the effect of different reflection coefficients, positive and negative, at geological boundaries. The equation used to calculate the reflectivity coefficient based on the density ( $\rho$ ) and velocity ( $V$ ) of the two different layers (layers 1 and 2) is also shown. (b) Reflectivity coefficient equation and range of density and velocity inputs used are based on Table 1. (c) Two examples of specific density and velocity inputs to the reflectivity coefficient equation that produce reflectivity coefficients close to those of Warner (1990) and Deemer and Hurich (1994). This demonstrates that strong reflectivity can theoretically be generated by these velocity and density scenarios, which are supported by both published data (Table 1) and gravity modelling (Fig. 7). We show the range of outputs for a strong positive reflectivity only (increase in impedance contrast); however, due to the phase rotation that may occur at such depths, it is possible that the reflections may also represent a decrease in the impedance contrast. If the high-amplitude reflections represent a decrease in the impedance contrast, then the values of reflectivity coefficient will be the same, but will be negative (e.g.  $-0.10$  and  $-0.16$ ). Source: part (a) modified from Cox *et al.* (2020).

crystalline crust, only one will be negative (decrease in impedance contrast) and the other positive (increase in impedance contrast). Figure 9 shows an example of calculating the reflectivity coefficient value for a positive impedance contrast only.

The combination of inputs ( $\rho_1$ ,  $\rho_2$ ,  $V_1$  and  $V_2$ ) that generates the strongest (highest) reflectivity coefficient output ( $\pm 0.25$ ) is 3500 kg m<sup>-3</sup> and 8500 m s<sup>-1</sup> for the lower crustal intrusions and 2750 kg m<sup>-3</sup> and 6000 m s<sup>-1</sup> for the crystalline crust. The high

density ( $3500 \text{ kg m}^{-3}$ ) and velocity ( $8500 \text{ m s}^{-1}$ ) inputs for the lower crustal intrusions are at the highest end of the published values (Table 1) and are therefore possibly less characteristic of lower crustal intrusions, particularly as the density ( $3500 \text{ kg m}^{-3}$ ) used for the lower crustal intrusions is higher than that of the published density ranges for the upper mantle ( $3200\text{--}3330 \text{ kg m}^{-3}$ , Table 1). The density of the lower crustal intrusions should be less than that of the mantle (to facilitate the propagation of magma through the upper mantle and into the crust; Cox 1980, 1993), but denser than the crystalline crust (i.e. between  $2750$  and  $3200 \text{ kg m}^{-3}$ ), for magma to stall and be emplaced within the lower crust (Cox 1980, 1993). We show two examples of velocity and density input combinations that produce theoretical reflectivity coefficient values between  $\pm 0.10$  and  $\pm 0.18$  (Fig. 9c), which are constrained to the published density and velocities values for both the crystalline crust and lower crustal intrusions (Table 1) while also honouring the process of emplacement described here. This demonstrates that it is possible for lower crustal intrusions (likely gabbroic in composition) emplaced within crystalline continental crust to theoretically generate reflectivity.

### 2D gravity modelling of lower crustal intrusions beneath the central-northern Corona Ridge

To determine whether an interpretation of lower crustal intrusions beneath the central-northern Corona Ridge is reasonable, four 2D gravity models were produced to test four different deep crustal geological interpretations. The base of the crystalline continental crust is taken as the base of the high-amplitude reflections and is kept the same within all four models. The tops of the crystalline continental crust and the sedimentary sections are also kept the same in all models.

Model A (Fig. 7a) includes no igneous intrusion within the lower crust. Predicted gravity values are low within the centre of the 2D line and are high towards the NE part of the 2D line compared with the observed gravity signal. Model A (Fig. 7a) is therefore not a suitable fit to the observed free air anomaly data.

Model B (Fig. 7b) consists of two sub-models. The high-amplitude reflections mapped within the 3D seismic reflection data (shown in red, Fig. 7b) were modelled first, then were modelled with the addition of unresolved disseminated igneous material (shown in black, Fig. 7b) below the seismic resolution. It is important to note that there is considerable uncertainty regarding both the distribution and geometry of the sub-seismic resolution intrusions. Both sub-models provide a suitable match to the observed free air anomaly data and the addition of unresolved material does not appear to considerably change the modelled gravity signal.

High-velocity lower crustal layers have been interpreted on refraction data along the NE Atlantic Margin. Model C (Fig. 7c) depicts the modelled gravity signal of a lower crustal layer with a high velocity ( $7500 \text{ m s}^{-1}$ ; see Table 1 and Fig. 4) at the Moho beneath the central-northern Corona Ridge and lacks the presence of any lower crustal intrusions. Much like model A, the predicted gravity values are too low within the centre of the 2D line and are too high towards the NE part of the 2D line when compared with the observed gravity signal. Model C does not provide a suitable match to the observed free air anomaly data and is not supported by the 3D seismic reflection data.

Model D (Fig. 7d) combines both the interpretation of lower crustal intrusions (model B) with the possible presence of a lower crustal layer (model C). The modelled gravity signal of model D is a suitable match to the observed free air anomaly data within the centre of the 2D line, but is a poor match along the NE section of the 2D line.

Overall, model B (both sub-models) and model D provide the best matches to observed free air anomaly data. Model D (Fig. 7d) incorporates a lower crustal layer that we see no evidence of within

the seismic reflection data, whereas model B (Fig. 7b) is more constrained to the seismic data. Model B, including the potential for significant unresolved disseminated igneous material, is therefore our preferred interpretation and estimates for the potential associated uplift are based on the geological interpretation shown in model B.

### Estimates for potentially associated uplift

Using the maximum thickness estimate of the lower crustal reflections ( $5.12 \text{ km}$ ; see Table 4) obtained from mapping the reflections in seismic data and including potentially unresolved material (see model B, Fig. 7b and Table 4) as an input into equation (1) (Brodie and White 1994, 1995), we estimate that the potential emplacement of up to  $5.12 \text{ km}$  of lower crustal intrusions may have resulted in an uplift of  $c. 310 \text{ m}$  along the central-northern Corona Ridge.

### Elevated present day geothermal gradients along the Corona Ridge

Within the FSB, geothermal gradients for 73 hydrocarbon exploration, appraisal and production wells shown within Figure 8a range between  $22.7^\circ\text{C km}^{-1}$  (well 214/29-1) and  $47.9^\circ\text{C km}^{-1}$  (well 213/25c-1V). The average geothermal gradient of the 73 wells is  $35.7^\circ\text{C km}^{-1}$ . Geothermal gradients of 11 hydrocarbon wells drilled along the Corona Ridge (located in quadrants 205, 213 and 214, Fig. 8a) range between  $34.3^\circ\text{C km}^{-1}$  (well 213/27-2) and  $47.9^\circ\text{C km}^{-1}$  (well 213/25c-1V). The average geothermal gradient along the Corona Ridge is  $41.4^\circ\text{C km}^{-1}$ , which is  $5.7^\circ\text{C km}^{-1}$  higher than the average geothermal gradient of the FSB and  $16.4^\circ\text{C km}^{-1}$  higher than the typical geothermal gradient of  $25^\circ\text{C km}^{-1}$  for continental crustal domains along passive margins (Allen and Allen 2013). The spatial relationship of the elevated geothermal gradients and high-amplitude lower crustal reflections is explored in the discussion section.

## Discussion

### Depth of the high-amplitude reflections beneath the central-northern Corona Ridge

Using 3D seismic reflection data, we mapped a series of high-amplitude reflections between  $14$  and  $20 \text{ km}$  depth ( $c. 7\text{--}9 \text{ s TWT}$ ) analogous (in geometry, reflectivity and depth) to published examples of crustal reflections interpreted as intrusions along the NE Atlantic Margin (see Smith *et al.* 2005; Cartwright and Hansen 2006; White *et al.* 2008, 2010; Abdelmalak *et al.* 2017; Wrona *et al.* 2019b). We have also shown that it is possible to generate strong reflections with reflectivity coefficients of  $\pm 0.16$  for lower crustal intrusions using published values for the densities and velocities of both lower crustal intrusions and the crystalline continental crust located along the NE Atlantic Margin (Fig. 9).

Mapping of the Moho shows that it varies between  $18$  and  $20 \text{ km}$  depth (Fig. 4), which is consistent with other published Moho depth ranges of  $17\text{--}20 \text{ km}$  (White *et al.* 2005; Makris *et al.* 2009; Roberts *et al.* 2009; Funck *et al.* 2016; Badley Geoscience Limited 2019; Fig. 1a) beneath the central-northern Corona Ridge. We therefore interpret that the high-amplitude reflections identified in this study are most likely located within the lower crust.

### Comparing lower crustal reflections beneath the Corona Ridge with analogous examples from the NE Atlantic Margin

Beneath the Fugloy Ridge, White *et al.* (2008) interpreted lower crustal intrusions on the 2D iSIMM Faroes profile (Fig. 2) between  $c. 6$  and  $7 \text{ s TWT}$  ( $c. 15 \text{ km}$  depth) (White *et al.* 2008, p. 461, their



fig. 2), *c.* 160 km to the NW of the igneous intrusions we interpreted beneath the central-northern Corona Ridge (Fig. 2). On the basis of their reflectivity, amplitude and geometry, we interpret the same reflections (*c.* 6–7 s TWT *c.* 160 km along the line in Fig. 2) as intrusions within the upper (not lower) continental crust, which possibly propagated into sequences T22–T35 (Selandian). We acknowledge that due to the thick volcanic pile (*c.* 3.5 s TWT) interpreted above the Fugloy Ridge (within sequences T22–T50, Fig. 2) (Jolley *et al.* 2021, p. 4, their fig. 2), sub-basalt imaging is challenging (Hardwick *et al.* 2010; Poppitt *et al.* 2018) and that the interpretation of deep structures becomes more uncertain and interpretations are likely to vary (Fig. 2; Smith *et al.* 2005; White *et al.* 2008, 2010). Nevertheless, the depth (*c.* 15 km, White *et al.* 2008, p. 461, their fig. 2b and 2c) at which the lower crustal intrusions are interpreted by White *et al.* (2008) is comparable with the depth of the lower crustal reflections interpreted within this study beneath the central-northern Corona Ridge (*c.* 14–20 km).

Beneath the Vøring Basin, *c.* 500 km NE of the central-northern Corona Ridge, Abdelmalak *et al.* (2017, p. 2505, their fig. 5) described numerous ‘rough’ high-amplitude reflections located at 7–10 s TWT, referred to as the T-reflection, which are analogous to those identified and described within this study. Also beneath the Vøring Basin, Cartwright and Hansen (2006, p. 931, their fig. 3) interpreted analogous high-amplitude reflections between 5 and 7 s TWT as sills intruded into crustal host rocks. Gernigon *et al.* (2003, 2004) described a high-velocity lower crustal dome marked by a high-amplitude reflection (the T-reflection) between 7 and 8 s TWT beneath the Gjallar Ridge within the Vøring Basin (Gernigon *et al.* 2004, p. 366, their fig. 4). Also at the Gjallar Ridge, Kilhams *et al.* (2021) (p. 15, their fig. 12) described the dome-like shape of the high-amplitude T-reflection beneath the Dalsnuten structure within the Vøring area. Although the T-reflection described by both Gernigon *et al.* (2003, 2004) and Kilhams *et al.* (2021) is not comprised of multiple rough reflections, the elongated dome-like structure of the T-reflection is comparable in geometry and depth (also 7–9 s TWT depth) with that which we have mapped beneath the central-northern Corona Ridge. Kilhams *et al.* (2021) suggested that the high-amplitude dome may represent the first stages of magmatic upwelling and development of a magma reservoir. Gernigon *et al.* (2004) does not assign a single interpretation of the high-velocity lower crustal dome and instead suggests five hypotheses for the nature of the crustal dome, including high-velocity sills. Mjelde *et al.* (2001, 2009) interpret a mafic intrusion related to the last phase of rifting as one possible origin of a high-velocity (7200–7600 m s<sup>-1</sup>) lower crustal layer with high-amplitude reflections at 15–25 km within the Vøring area, also consistent with the depths at which we map the lower crustal reflections beneath the central-northern Corona Ridge (*c.* 14–20 km).

In the Møre Basin, 400 km NE of the central-northern Corona Ridge, Peron-Pinvidic *et al.* (2022, p. 3, their fig. 2) describe a series of deep high-amplitude reflections present within the lower crust, typically at depths of 9–11 s TWT, and suggest multiple interpretations of these reflections, including shear zones and magma intrusions. The reflections described by Peron-Pinvidic *et al.* (2022) are analogous to those described in this study and by Cartwright and Hansen (2006) and Abdelmalak *et al.* (2017).

In the Central North Sea, Lyngsie and Thybo (2007) interpret magmatic intrusive complexes within the lower crust beneath the central graben, the Mid North Sea High and the Horn Graben based on reflection and refraction data. Within the Northern North Sea, *c.* 800 km east from the Corona Ridge, analogous lower crustal reflectivity (in depths, geometries and reflectivity) is interpreted as an extensive igneous sill in the lower crust (Wrona *et al.* 2019b) and a layered lower crust (McBride *et al.* 2004, p. 4, their fig. 3).

If the lower crustal reflections we mapped beneath the Corona Ridge are lower crustal intrusions, then they would represent just

one small component of the NAIP deep crustal plumbing system. Inboard (closer to the continental shelf), petrological, geochemical and seismic evidence suggest that igneous intrusions and high-velocity layers were emplaced as deep crustal magma reservoirs within the continental crystalline crust and at the Moho during periods of Paleogene magmatism (Central Viking Graben, Lyngsie and Thybo 2007; Northern North Sea, Wrona *et al.* 2019b; British Isles, Brodie and White 1994, 1995; Chambers and Fitton 2000; Maclennan and Lovell 2002; FSB, this study; Faroe Islands, Richardson *et al.* 1998; Vøring Basin, Mjelde *et al.* 2001, 2009; Gernigon *et al.* 2003; Cartwright and Hansen 2006; Abdelmalak *et al.* 2017). Outboard, the presence of seaward-dipping reflections suggests that the crust is magmatic (this study, Fig. 2; White *et al.* 2008, p. 461, their fig. 2; Abdelmalak *et al.* 2015, p. 1012, their fig. 2 and references cited therein), with similar features also observed outboard at Hatton Bank (Smith *et al.* 2005; White *et al.* 2008, 2010). Although we interpret only minor crustal intrusions into the magmatic crustal domain (Fig. 2), the thick volcanic pile present along the Fugloy Ridge (Fig. 2) may potentially be impeding our ability to detect and resolve further lower crustal intrusions and/or other geological features.

We acknowledge that the interpretation of igneous intrusions, whether emplaced within sedimentary sections or the crust, presents significant challenges. Over-migration of seismic data may also complicate the true geometries of the lower crustal intrusions that may be present because upward-curving diffractions at the edge of reflections may produce the appearance of an intrusion ‘tip’ (Hansen *et al.* 2004). As a result, the more detailed geometries of the high-amplitude reflections (Fig. 5), and any geometries observed at these depths (7–9 s TWT) within the published literature, may not be an accurate representation of the actual geometry present and, as a result, should be interpreted with caution and alongside other methods of identification and analysis (e.g. gravity modelling).

### ***Other possible interpretations of the high-amplitude lower crustal reflections***

Ductile shear zones have been discussed as a potential cause of lower crustal reflectivity both along the NE Atlantic Margin (Reston 1988; Wrona *et al.* 2019a; Peron-Pinvidic *et al.* 2022) and in the southern Atlantic (Clerc *et al.* 2015). The geometries of the lower crustal reflections (Figs 4, 5) are more comparable to igneous intrusions emplaced within sedimentary basins (e.g. Hansen *et al.* 2004; Schofield *et al.* 2017; Mark *et al.* 2018b) than the typical geometries associated with shear zones (Reston 1988; Clerc *et al.* 2015). According to Warner (1990), the reflectivity coefficient values of bright lower crustal reflections (>0.1) are also generally much larger than the reflectivity coefficient values of most shear zones. Although we have provided evidence to support the view that the high-amplitude lower crustal reflections beneath the central-northern Corona Ridge are more likely to correspond to igneous intrusions, we cannot fully exclude the presence of shear zones as an alternative interpretation.

### ***Lower crustal intrusion beneath the Corona Ridge: a realistic estimate?***

The cumulative thickness estimates for the lower crustal reflections mapped in this study (0.65–5.12 km; Table 4) are comparable with the 1–5 km ‘underplate’ thickness range estimates published for the FSB, which are based primarily on subsidence modelling (Clift 1997; Nadin *et al.* 1997; White and Lovell 1997). Specifically, our upper thickness estimates for the lower crustal reflections are comparable with the 3–4 km estimate proposed by Clift and Turner (1998) for magmatic underplating beneath the central FSB Corona Ridge area, but are comparatively low when compared with those for the Hatton–

Rockall and Vøring regions (up to 15 km; [Hinz \*et al.\* 1987](#); [White \*et al.\* 1987](#); [Mjelde \*et al.\* 2001, 2009](#); [Smith \*et al.\* 2005](#)).

The volumes estimated for the lower crustal igneous sill interpreted by [Wrona \*et al.\* \(2019b\)](#) ( $472 \pm 161 \text{ km}^3$ ) beneath the Northern North Sea and the lower crustal intrusions interpreted beneath the Fugloy Ridge by [Roberts \*et al.\* \(2009\)](#) ( $560\text{--}780 \text{ km}^3$ ) are comparable with the volume we estimated for the lower crustal reflections beneath the central-northern Corona Ridge when not taking into account the potential of unresolved igneous material ( $111\text{--}888 \text{ km}^3$ ; [Table 4](#)). We estimate the potential volume of lower crustal intrusions to be between 266 and  $2131 \text{ km}^3$  (when accounting for potentially unresolved material) based on the mapping of a series of high-amplitude reflections within the lower crust beneath the central-northern Corona Ridge.

### ***Do elevated present day geothermal gradients support the presence of lower crustal intrusions?***

Where crustal intrusions have been interpreted along the NE Atlantic Margin (e.g. the Norwegian Basin; [Smith \*et al.\* 2005](#); [White \*et al.\* 2008, 2010](#); the Vøring Basin, [Mjelde \*et al.\* 2001](#); [Cartwright and Hansen 2006](#); [Abdelmalak \*et al.\* 2017](#); and the Northern North Sea, [Wrona \*et al.\* 2019b](#)), there are relatively few wells that can provide constraints on the present day geothermal gradients in relation to the potential presence of lower crustal intrusions. Elevated present day geothermal gradients have, however, been associated with magmatic addition into the crust in other tectonic settings (e.g. the Central Asian Orogenic Belt, [Xu \*et al.\* 2021](#); the Ribeira Fold Belt, [Bento dos Santos \*et al.\* 2010](#)). The rise in continental geothermal gradients attributed to Paleogene magmatic underplating ([Fyfe 1992](#)) and the possible ongoing present day thermal effects still caused by a thermal anomaly ([Fernández \*et al.\* 2004](#)) or magmatic underplating ([Fjeldskaar \*et al.\* 1999](#); [Kilhams \*et al.\* 2022](#)) have been discussed along the NE Atlantic Margin. However, the thermal influence from lower crustal intrusions that may have occurred along the NE Atlantic Margin is likely to have long decayed and is unlikely to still affect the present day heat flow ([Clift 1999](#); [Ritter \*et al.\* 2004](#)).

Elevated geothermal gradients may also be attributed to a residual isostatic or thermal anomaly ([Smallwood 2008](#); [Fletcher \*et al.\* 2013](#); [Ripington \*et al.\* 2015](#)), the heterogeneous radiogenic content of the crystalline continental crust within the FSB ([APT & Chemostrat 2021](#)) or the presence of igneous intrusions that have been emplaced into sedimentary sequences ([Persano \*et al.\* 2007](#); [Holford \*et al.\* 2013](#)), although the latter is unlikely because there is a lack of intrusions emplaced within sedimentary sequences overlying the basement-cored ridge ([Figs 2, 4 and 6](#); see also [Layfield \*et al.\* 2022](#)). It is therefore not clear whether elevated present day geothermal gradients support an interpretation of lower crustal intrusions beneath the Corona Ridge. However, if lower crustal intrusions were emplaced beneath the Corona Ridge, then the thermal effects during and after magma emplacement are an important (and, according to [Fjeldskaar \*et al.\* 1999](#), significant) variable to consider when modelling hydrocarbon generation and expulsion within regional basin models and along the NE Atlantic Margin as a whole (see [Clift 1997](#); [Clift and Turner 1998](#); [Carr and Scotchman 2003](#); [White \*et al.\* 2010](#); [Wangen \*et al.\* 2011](#); [Cunha \*et al.\* 2021](#); [Gac \*et al.\* 2021](#); [Kilhams \*et al.\* 2022](#)). [Gardiner \*et al.\* \(2019\)](#) demonstrated the importance of using the correct basement radiogenic heat production within basin models along the Corona Ridge area and how this can influence the onset of petroleum expulsion. It may therefore be important to consider how the potential addition of a substantial amount of basic (gabbroic) igneous material to the lower crust beneath the Corona Ridge may have altered the radiogenic heat production and bulk thermal conductivity of the crust after emplacement.

### ***Potential implications for basins located along the NE Atlantic Margin***

The addition of magma within the lower crust and at the Moho has been linked to Paleogene uplift and the subsequent deposition of Paleocene–Eocene sequences within the NE Atlantic region ([Brodie and White 1994, 1995](#); [White 1997](#); [White and Lovell 1997](#); [Clift and Turner 1998](#); [Naylor \*et al.\* 1999](#); [Jones \*et al.\* 2002](#); [MacLennan and Lovell 2002](#); [Tiley \*et al.\* 2004](#); [Rudge \*et al.\* 2008](#); [Smallwood 2008](#)), although work focused on estimating the permanent uplift potentially caused by magmatic underplating within the region are sparse. Estimates of the distribution, magnitude and chronology of Paleogene uplift have generally been focused on constraining transient uplift within the FSB ([Smallwood and Gill 2002](#); [Shaw-Champion \*et al.\* 2008](#); [Hartley \*et al.\* 2011](#); [Hardman \*et al.\* 2018b](#)).

[Shaw-Champion \*et al.\* \(2008\)](#) argued that for Paleogene uplift to be generated by the emplacement of magma within the lower crust, several kilometres of magmatic underplating would be required. We have provided evidence to suggest that  $>5 \text{ km}$  of igneous material may be present within the lower crust beneath the central-northern Corona Ridge, which is consistent with estimates published previously ([Clift 1997](#); [White and Lovell 1997](#); [Clift and Turner 1998](#)). The estimate proposed by this study of *c.* 310 m of permanent uplift, which may have been generated by the potential emplacement of the high-amplitude reflections as intrusions, is consistent with [Brodie and White \(1995\)](#) and [Clift and Turner \(1998\)](#), who proposed that widespread magmatic underplating of 1–5 km within the FSB generated permanent uplift of several hundred metres.

Distinguishing what proportion of the total Paleogene uplift recorded within the FSB was generated by a thermal anomaly ([Nadin \*et al.\* 1997](#); [White 1997](#); [White and Lovell 1997](#); [Jones \*et al.\* 2002](#); [Rudge \*et al.\* 2008](#); [Shaw-Champion \*et al.\* 2008](#); [Hartley \*et al.\* 2011](#); [Hardman \*et al.\* 2018b](#)), the emplacement of magma at the Moho and within the lower crust ([Brodie and White 1994, 1995](#); [White and Lovell 1997](#); [Jones \*et al.\* 2002](#); [MacLennan and Lovell 2002](#); [Tiley \*et al.\* 2004](#); [Smallwood 2008](#)) or a change in tectonic regime ([Ellis and Stoker 2014](#); [Mudge 2015](#); [Jolley \*et al.\* 2021](#)) is challenging due to the difficulty in constraining the uplift and subsidence histories of the basin ([Shaw-Champion \*et al.\* 2008](#)). It may be possible that a few hundred metres (e.g. the 310 m proposed in this study, [Brodie and White 1995](#) and [Clift and Turner 1998](#)) of the total Paleogene uplift was generated along the Corona Ridge by the permanent uplift caused by crustal thickening generated by the emplacement of lower crustal intrusions (see [Brodie and White 1994, 1995](#); [Allen and Allen 2013](#)) and the rest by other mechanisms.

The potential implications of 310 m of uplift are also an important consideration for reservoir play fairways due to the significant amount of sediment possibly being shed into the areas surrounding the Corona Ridge as a result of uplift. The integration of our results with a more detailed understanding of the distribution, magnitude and chronology of Paleogene uplift along the central-northern Corona Ridge could improve our understanding of the potential role that lower crustal intrusion may have had in Paleogene uplift and the subsequent clastic input into the FSB.

### **Conclusions**

In contrast with the rest of the NE Atlantic Margin, where seismic reflectivity ascribed to lower crustal intrusions has been documented, analogous lower crustal intrusion within the FSB had hitherto been speculated based on non-seismic evidence (e.g. Paleogene uplift and heat flow) and modelling. Previous work proposed emplaced igneous thicknesses of 1–5 km within the lower crust and/or at the Moho in this region, with some arguing that the observed



Paleogene uplift would have required several kilometres of magma emplacement at the Moho and/or within the lower crust. Using broadband 3D seismic reflection data, we have provided evidence strongly supporting the presence of lower crustal intrusions beneath the central-northern Corona Ridge by mapping a series of deep (14–20 km depth) high-amplitude lower crustal reflections. We propose the following.

- It is theoretically possible to generate a strong reflection coefficient using published values for the densities and velocities of both lower crustal intrusions and crystalline continental crust located along the NE Atlantic Margin.
- The cumulative thickness of the high-amplitude reflections may be >5 km in places. This value is consistent with previous estimates derived from geochemical and petrological studies in the region. If the high-amplitude reflections represent lower crustal intrusions, then a substantial amount of igneous material may be present beneath the Corona Ridge.
- If the lower crustal high-amplitude reflections represent lower crustal intrusions, then their presence provides a potential mechanism by which Paleogene uplift may have taken place.
- Volumetric estimates of the high-amplitude reflections beneath the central-northern Corona Ridge, when also accounting for potentially unresolved igneous material, are estimated to be between *c.* 266 and 2131 km<sup>3</sup>.
- The modelled 2D gravity signature of the interpretation of lower crustal intrusions beneath the Corona Ridge provides a suitable match to the observed free air gravity anomaly data.
- The potential emplacement of lower crustal intrusions added to the crust beneath the Corona Ridge by the accretion of gabbroic magma during the Paleogene may also be responsible for a significant amount of Paleogene uplift of >300 m.

Our results provide new insights into the possible deep crustal structure of the FSB and should prove valuable to further work linking lower crustal intrusions to their impacts on basinal heat flow and the subsequent generation and expulsion of petroleum, the associated Paleogene uplift and the subsequent Paleocene–Eocene clastic input within the FSB. Further work to increase the understanding of the distribution, magnitude and chronology of Paleogene uplift along the central-northern Corona Ridge, and within the FSB as whole, should be undertaken to assess the true role that lower crustal intrusion may have had in controlling Paleogene vertical motion in this region.

*Scientific editing by Giovanni Camanni*

**Acknowledgements** This paper forms part of the lead author's PhD research conducted as part of the Natural Environment Research Council Centre for Doctoral Training in Oil and Gas at the University of Aberdeen. WesternGeco are thanked for providing access to the WesternGeco Multiclient 2D iSIMM Faroes profile (Fig. 2) and for granting permission to publish this profile. This paper contains information provided by the North Sea Transition Authority and/or other third parties. PGS are thanked for the generous provision of the MegaSurveyPlus seismic dataset to the PhD project. Seismic interpretation was undertaken using Schlumberger Petrel and IHS Kingdom software, respectively, using academic licences kindly provided by Schlumberger, which are gratefully acknowledged. ARK CLS are also acknowledged for providing academic licences to the XField Petrel plug-in. MW acknowledges valuable discussion and insight offered by the late, K.G. Cox regarding uplift of the Western Ghats (India) and during the preparation of Cox (1993). Thanks to Nick Kuszniir and Ken McDermott for constructive comments during the preparation of this paper. Joe Cartwright, Christopher Jackson and an anonymous reviewer are thanked for their constructive and detailed reviews, which improved this paper.

**Author contributions** LKL: conceptualization (lead), data curation (lead), formal analysis (lead), investigation (lead), methodology (lead),

visualization (lead), writing – original draft (lead), writing – review and editing (lead); NS: conceptualization (supporting), data curation (supporting), supervision (lead), visualization (supporting), writing – original draft (supporting), writing – review and editing (supporting); DW: conceptualization (supporting), visualization (supporting), writing – review and editing (supporting); SPH: data curation (supporting), writing – review and editing (supporting); DWJ: writing – review and editing (supporting); BAK: writing – review and editing (supporting); DKM: writing – review and editing (supporting); AMR: writing – review and editing (supporting); ADA: writing – review and editing (supporting); AE: writing – review and editing (supporting); MW: writing – review and editing (supporting).

**Funding** This work was funded by the University of Aberdeen (RT10121-14), the Natural Environment Research Council Centre for Doctoral Training in Oil and Gas (NE/M00578X/1) and Total E&P UK Limited (RG14991). Principal award recipient: Lucinda Kate Layfield.

**Competing interests** The authors declare that they have no known competing financial interests or personal relationships that could have appeared to influence the work reported in this paper.

**Data availability** The main data that support the findings of this study (Galloway/Corona 3D, survey names TT133-D0003 and TT153-D0002) are available from the North Sea Transition Authority National Data Repository (NSTA NDR) (<https://ndr.nstauthority.co.uk/>), along with the acquisition and processing reports for both surveys. Restrictions apply to the availability of the WesternGeco Multiclient 2D iSIMM Faroes profile data, which were used under permission for the current study and are not publicly available. The 2D seismic data used (not shown in this paper) to extrapolate volcanic sequences from Brudgen exploration wells (6104/21-1 and 6104/21-2) to the 2D iSIMM Faroes profile are available from Jarðfeingi, the Faroese Geological Survey (<https://jf.fo/en/datur/seismikk-datur/>). The well data used throughout this paper are freely available and can be downloaded from the NSTA NDR portal. The gravity data used as part of this study (WGM 2012 Global Model) are publicly available from the International Gravimetric Bureau (<https://bgi.obs-mip.fr/data-products/grids-and-models/wgm2012-global-model/>). The geothermal data used within this study are freely available from the NSTA Open Data site (<https://opendata-nstauthority.hub.arcgis.com/documents/NSTAAUTHORITY::cgg-geothermal-database/about>), but this does not include wells located along the Corona Ridge (see Fig. 8a).

## References

- Abdelmalak, M.M., Andersen, T.B. *et al.* 2015. The ocean–continent transition in the mid-Norwegian margin: insight from seismic data and an onshore Caledonian field analogue. *Geology*, **43**, 1011–1014, <https://doi.org/10.1130/G37086.1>
- Abdelmalak, M.M., Faleide, J.I., Planke, S., Gernigon, L., Zastozhnov, D., Shephard, G.E. and Myklebust, R. 2017. The T-reflection and the deep crustal structure of the Vøring Margin, offshore Mid-Norway. *Tectonics*, **36**, 2497–2523, <https://doi.org/10.1002/2017TC004617>
- Allen, P.A. and Allen, J.R. 2013. *Basin Analysis: Principles and Application to Petroleum Play Assessment*. Wiley, Chichester.
- Alvey, A., Gaina, C., Kuszniir, N.J. and Torsvik, T.H. 2008. Integrated crustal thickness mapping and plate reconstructions for the high Arctic. *Earth and Planetary Science Letters*, **274**, 310–321, <https://doi.org/10.1016/j.epsl.2008.07.036>
- Applied Petroleum Technology (APT) (UK) Ltd & Chemostrat Ltd 2021. *Faroe–Shetland Basin Basement Characterisation and Thermal Calibration Database & Report*, <https://hub.arcgis.com/documents/NSTAAUTHORITY::apt-chemostrat-faroe-shetland-basin-basement-characterisation-and-thermal-calibration-database-report/about>
- Badley Geoscience Limited 2019. *OCTek-UK Report*. North Sea Transition Authority Open Data, <https://opendata-nstauthority.hub.arcgis.com/documents/NSTAAUTHORITY::octek-uk/about>
- Balmino, G., Vales, N., Bonvalot, S. and Briais, A. 2011. Spherical harmonic modelling to ultra-high degree of Bouguer and isostatic anomalies. *Journal of Geodesy*, **86**, 499–520, <https://doi.org/10.1007/s00190-011-0533-4>
- Bento dos Santos, T.M., Munhá, J.M., Tassinari, C.C.G., Fonseca, P.E. and Dias Neto, C. 2010. Thermochronology of central Ribeira Fold Belt, SE Brazil: petrological and geochronological evidence for long-term high temperature maintenance during Western Gondwana amalgamation. *Precambrian Research*, **180**, 285–298, <https://doi.org/10.1016/j.precamres.2010.05.002>
- Brodie, J. and White, N. 1994. Sedimentary basin inversion caused by igneous underplating: northwest European continental shelf. *Geology*, **22**, 147–150, [https://doi.org/10.1130/0091-7613\(1994\)022%3C0147:SBICBI%3E2.3.CO;2](https://doi.org/10.1130/0091-7613(1994)022%3C0147:SBICBI%3E2.3.CO;2)
- Brodie, J. and White, N. 1995. The link between sedimentary basin inversion and igneous underplating. *Geological Society, London, Special Publications*, **88**, 21–38, <https://doi.org/10.1144/GSL.SP.1995.088.01.03>

- Carr, A.D. and Scotchman, I.C. 2003. Thermal history modelling in the southern Faeroe–Shetland Basin. *Petroleum Geoscience*, **9**, 333–345, <https://doi.org/10.1144/1354-079302-494>
- Cartwright, J. and Hansen, D.M. 2006. Magma transport through the crust via interconnected sill complexes. *Geology*, **34**, 929–932, <https://doi.org/10.1130/G22758A.1>
- Chadwick, R.A. and Pharaoh, T.C. 1998. The seismic reflection Moho beneath the United Kingdom and adjacent areas. *Tectonophysics*, **299**, 255–279, [https://doi.org/10.1016/S0040-1951\(98\)00193-0](https://doi.org/10.1016/S0040-1951(98)00193-0)
- Chambers, L.M. and Fitton, J.G. 2000. Geochemical transitions in the ancestral Iceland plume: evidence from the Isle of Mull Tertiary volcano, Scotland. *Journal of the Geological Society, London*, **157**, 261–263, <https://doi.org/10.1144/jgs.157.2.261>
- Chappell, A.R. and Kusznir, N.J. 2008. Three-dimensional gravity inversion for Moho depth at rifted continental margins incorporating a lithosphere thermal gravity anomaly correction. *Geophysical Journal International*, **174**, 1–13, <https://doi.org/10.1111/j.1365-246X.2008.03803.x>
- Christensen, N.I. and Mooney, W.D. 1995. Seismic velocity structure and composition of the continental crust: a global view. *Journal of Geophysical Research*, **100**, 9761–9788, <https://doi.org/10.1029/95JB00259>
- Clerc, C., Jolivet, L. and Ringenbach, J.-C. 2015. Ductile extensional shear zones in the lower crust of a passive margin. *Earth and Planetary Science Letters*, **431**, 1–7, <https://doi.org/10.1016/j.epsl.2015.08.038>
- Clift, P.D. 1991. The thermal impact of Paleocene magmatic underplating in the Faeroe–Shetland–Rockall region. *Geological Society, London, Petroleum Geology Conference Series*, **5**, 585–593, <https://doi.org/10.1144/0050585>
- Clift, P.D. 1997. Temperature anomalies under the northeast Atlantic rifted volcanic margins. *Earth and Planetary Science Letters*, **146**, 195–211, [https://doi.org/10.1016/S0012-821X\(96\)00228-2](https://doi.org/10.1016/S0012-821X(96)00228-2)
- Clift, P.D. and Turner, J. 1998. Paleogene igneous underplating and subsidence anomalies in the Rockall–Faeroe–Shetland area. *Marine and Petroleum Geology*, **15**, 223–243, [https://doi.org/10.1016/S0264-8172\(97\)00056-1](https://doi.org/10.1016/S0264-8172(97)00056-1)
- Clift, P.D. 1999. The thermal impact of Paleocene magmatic underplating in the Faeroe–Shetland–Rockall region. *Geological Society, London, Petroleum Geology Conference Series*, **5**, 585–593, <https://doi.org/10.1144/0050585>
- Cox, K.G. 1980. A model for flood basalt volcanism. *Journal of Petrology*, **21**, 629–650, <https://doi.org/10.1093/petrology/21.4.629>
- Cox, K.G. 1993. Continental magmatic underplating. *Philosophical Transactions of the Royal Society of London. Series A: Physical and Engineering Sciences*, **342**, 155–166, <https://doi.org/10.1098/rsta.1993.0011>
- Cox, D.R., Newton, A.M.W. and Huuse, M. 2020. Chapter 22 – An introduction to seismic reflection data: acquisition, processing and interpretation. In: Scarselli, N., Adam, J., Chiarella, D., Roberts, D.G. and Bally, A.W. (eds) *Regional Geology and Tectonics. Volume 1: Principles of Geologic Analysis*. 2nd edn. Elsevier, 571–603, <https://doi.org/10.1016/B978-0-444-64134-2.00020-1>
- Cunha, T.A., Rasmussen, H., Villinger, H. and Akinwumiji, A.A. 2021. Burial and heat flux modelling along a Southern Vøring basin transect: implications for the petroleum systems and thermal regimes in the deep Mid-Norwegian Sea. *Geosciences*, **11**, 190, <https://doi.org/10.3390/geosciences11050190>
- Deemer, S.J. and Hurich, C.A. 1994. The reflectivity of magmatic underplating using the layered mafic intrusion analog. *Tectonophysics*, **232**, 239–255, [https://doi.org/10.1016/0040-1951\(94\)90087-6](https://doi.org/10.1016/0040-1951(94)90087-6)
- Doré, A.G., Lundin, E.R., Fichler, C. and Olesen, O. 1997. Patterns of basement structure and reactivation along the NE Atlantic margin. *Journal of the Geological Society, London*, **154**, 85–92, <https://doi.org/10.1144/gsjgs.154.1.0085>
- Doré, A.G., Lundin, E.R., Jensen, L.N., Birkeland, Ø., Eliassen, P.E. and Fichler, C. 1999. Principal tectonic events in the evolution of the northwest European Atlantic margin. *Geological Society, London, Petroleum Geology Conference Series*, **5**, 41–61, <https://doi.org/10.1144/0050041>
- Eccles, J.D., White, R.S. and Christie, P.A.F. 2011. The composition and structure of volcanic rifted continental margins in the North Atlantic: further insights from shear waves. *Tectonophysics*, **508**, 22–33, <https://doi.org/10.1016/j.tecto.2010.02.001>
- Ellis, D. and Stoker, M.S. 2014. The Faeroe–Shetland Basin: a regional perspective from the Paleocene to the present day and its relationship to the opening of the North Atlantic Ocean. *Geological Society, London, Special Publications*, **397**, 11–31, <https://doi.org/10.1144/SP397.1>
- Ellis, D., Passey, S.R., Jolley, D.W. and Bell, B.R. 2009. Transfer zones: the application of new geological information from the Faeroe Islands applied to the offshore exploration of intra and sub-basalt strata. In: Ziska, H. and Varming, T. (eds) *Faeroe Islands Exploration Conference: Proceedings of the 2nd Conference*. Faeroese Society of Sciences and Humanities, Tórshavn, 205–226.
- Ernst, R.E. 2014. *Large Igneous Provinces*. Cambridge University Press, Cambridge.
- Fernández, M., Tome, M., Garcia-Castellanos, D., Vergés, J., Wheeler, W. and Karpuz, R. 2004. Deep structure of the Vøring Margin: the transition from a continental shield to a young oceanic lithosphere. *Earth and Planetary Science Letters*, **221**, 131–144, [https://doi.org/10.1016/S0012-821X\(04\)00092-5](https://doi.org/10.1016/S0012-821X(04)00092-5)
- Fjeldskaar, W., Johansen, H., Dodd, T.A. and Thompson, M. 1999. Temperature and maturity effects of magmatic underplating in the Gjallar Ridge, Norwegian sea. In: Förster, A. and Merriam, D.F. (eds) *Geothermics in Basin Analysis. Computer Applications in the Earth Sciences*. Springer, Boston, 131–149, [https://doi.org/10.1007/978-1-4615-4751-8\\_7](https://doi.org/10.1007/978-1-4615-4751-8_7)
- Fletcher, R., Kusznir, K., Roberts, A. and Hunsdale, R. 2013. The formation of a failed continental breakup basin: the Cenozoic development of the Faeroe–Shetland Basin. *Basin Research*, **25**, 532–553, <https://doi.org/10.1111/bre.12015>
- Funck, T., Hopper, J.R. *et al.* 2014. Chapter 6: Crustal structure. In: Hopper, J.R., Funck, T., Stoker, M., Ártung, U., Peron-Pinvidic, G., Doornenbal, H. and Gaina, C. (eds) *Tectonostratigraphic Atlas of the North-East Atlantic Region*. Geological Survey of Denmark and Greenland, Copenhagen, 69–126.
- Funck, T., Erlendsson, Ö., Geissler, W.H., Gradmann, S., Kimbell, G.S., McDermott, K. and Petersen, U.K. 2016. A review of the NE Atlantic conjugate margins based on seismic refraction data. *Geological Society, London, Special Publications*, **447**, 171–205, <https://doi.org/10.1144/SP447.9>
- Funck, T., Geissler, W.H., Kimbell, G.S., Gradmann, S., Erlendsson, Ö., McDermott, K. and Petersen, U.K. 2017. Moho and basement depth in the NE Atlantic Ocean based on seismic refraction data and receiver functions. *Geological Society, London, Special Publications*, **447**, 207–231, <https://doi.org/10.1144/SP447.1>
- Furlong, K.P. and Fountain, D.M. 1986. Continental crustal underplating: thermal considerations and seismic–petrologic consequences. *Journal of Geophysical Research*, **91**, 8285–8294, <https://doi.org/10.1029/JB091iB08p08285>
- Fyfe, W.S. 1992. Magma underplating of continental crust. *Journal of Volcanology and Geothermal Research*, **50**, 33–40, [https://doi.org/10.1016/0377-0273\(92\)90035-C](https://doi.org/10.1016/0377-0273(92)90035-C)
- Gac, S., Abdelmalak, M.M., Faleide, J.I., Schmid, D.W. and Zastrozhnov, D. 2021. Basin modelling of a complex rift system: the Northern Vøring Volcanic Margin case example. *Basin Research*, **34**, 702–726, <https://doi.org/10.1111/bre.12637>
- Gardiner, D., Schofield, N. *et al.* 2019. Modeling petroleum expulsion in sedimentary basins: the importance of igneous intrusion timing and basement composition. *Geology*, **47**, 904–908, <https://doi.org/10.1130/G46578.1>
- Geoffroy, L. 2005. Volcanic passive margins. *Comptes Rendus Geoscience*, **337**, 1395–1408, <https://doi.org/10.1016/j.crte.2005.10.006>
- Gernigon, L., Ringenbach, J.C., Planke, S., Le Gall, B. and Jonquet-Kolstø, H. 2003. Extension, crustal structure and magmatism at the outer Vøring Basin, Norwegian margin. *Journal of the Geological Society, London*, **160**, 197–208, <https://doi.org/10.1144/0016-764902-055>
- Gernigon, L., Ringenbach, J.-C., Planke, S. and Le Gall, B. 2004. Deep structures and breakup along volcanic rifted margins: insights from integrated studies along the outer Vøring Basin (Norway). *Marine and Petroleum Geology*, **21**, 363–372, <https://doi.org/10.1016/j.marpetgeo.2004.01.005>
- Greater London Authority 2018. *Land Area and Population Density, Ward and Borough*. <https://data.london.gov.uk/dataset/land-area-and-population-density-ward-and-borough>
- Hansen, D.M., Cartwright, J.A. and Thomas, D. 2004. 3D seismic analysis of the geometry of igneous sills and sill junctions. *Geological Society, London, Memoirs*, **29**, 199–208, <https://doi.org/10.1144/GSL.MEM.2004.029.01.19>
- Hansen, J., Davidson, J., Jerram, D., Ottley, C. and Widdowson, M. 2019. Contrasting TiO<sub>2</sub> compositions in early Cenozoic mafic sills of the Faeroe Islands: an example of basalt formation from distinct melting regimes. *Earth Sciences*, **8**, 235–267, <https://doi.org/10.11648/j.earth.20190805.11>
- Hardman, J., Schofield, N., Jolley, D., Hartley, A., Holford, S. and Watson, D. 2018a. Controls on the distribution of volcanism and intra-basaltic sediments in the Cambo-Rosebank region, west of Shetland. *Petroleum Geoscience*, **25**, 71–89, <https://doi.org/10.1144/petgeo2017-061>
- Hardman, J.P.A., Schofield, N. *et al.* 2018b. Prolonged dynamic support from the Icelandic plume of the NE Atlantic margin. *Journal of the Geological Society, London*, **175**, 396–410, <https://doi.org/10.1144/jgs2017-088>
- Hardwick, A., Travis, T., Stokes, S. and Hart, M. 2010. Lows and highs: using low frequencies and improved velocity tools to image complex ridges and basement highs in the Faeroe–Shetland Basin. *First Break*, **28**, 61–67, <https://doi.org/10.3997/1365-2397.28.9.41392>
- Hartley, R.A., Roberts, G.G., White, N. and Richardson, C. 2011. Transient convective uplift of an ancient buried landscape. *Nature Geoscience*, **4**, 562–565, <https://doi.org/10.1038/ngeo1191>
- Hinz, K., Mutter, J.C., Zehnder, C.M. and NGT Study Group 1987. Symmetric conjugation of continent–ocean boundary structures along the Norwegian and East Greenland margins. *Marine and Petroleum Geology*, **3**, 166–187, [https://doi.org/10.1016/0264-8172\(87\)90043-2](https://doi.org/10.1016/0264-8172(87)90043-2)
- Hitchen, K. and Ritchie, J.D. 1987. Geological review of the West Shetland area. In: Brooks, J. and Glennie, K.W. (eds) *Petroleum Geology of North West Europe, Vol. 2*. Graham and Trotman Limited, London, 737–749.
- Holdsworth, R.E., Morton, A. *et al.* 2019. The nature and significance of the Faeroe–Shetland Terrace: linking Archaean basement blocks across the North Atlantic. *Precambrian Research*, **321**, 154–171, <https://doi.org/10.1016/j.precamres.2018.12.004>
- Holford, S., Schofield, N., Jackson, C.A.-L., Magee, C., Green, P.F. and Duddy, I.R. 2013. Impacts of igneous intrusions on source and reservoir potential in prospective sedimentary basins along the Western Australian continental margin. Paper presented at the West Australian Basins Symposium 2013, 18–21 August, Perth, Australia, <https://archives.datapages.com/data/petroleum-exploration-society-of-australia/conferences/043/043001/pdfs/26.htm>



- Hughes, S., Barton, P.J. and Harrison, D.J. 1997. Characterizing the Mid-Faeroe Ridge using seismic velocity measurements. *Journal of Geophysical Research: Solid Earth*, **102**, 7837–7847, <https://doi.org/10.1029/96JB03809>
- Jolley, D.W. and Bell, B.R. 2002. The evolution of the North Atlantic Igneous Province and the opening of the NE Atlantic rift. *Geological Society, London, Special Publications*, **197**, 1–13, <https://doi.org/10.1144/GSL.SP.2002.197.01.01>
- Jolley, D.W., Millett, J.M., Schofield, N., Broadley, L. and Hole, M.J. 2021. Stratigraphy of volcanic rock successions of the North Atlantic rifted margin: the offshore record of the Faroe Shetland and Rockall basins. *Earth and Environmental Science Transactions of the Royal Society of Edinburgh*, **112**, 61–88, <https://doi.org/10.1017/S1755691021000037>
- Jones, S.M., White, N., Clarke, B.J., Rowley, E. and Gallagher, K. 2002. Present and past influence of the Iceland Plume on sedimentation. *Geological Society, London, Special Publications*, **196**, 13–25, <https://doi.org/10.1144/GSL.SP.2002.196.01.02>
- Joseph, S., Lu, X., Bykov, K. and Douillard, A. 2017. Extensive broadband 3-D seismic to de-risk and mature the West of Shetland exploration portfolio. *79th EAGE Conference and Exhibition*, 12–15 June, Paris, France, European Association of Geoscientists & Engineers, 1–5, [earthdoc.org/content/papers/10.3997/2214-4609.201700816](http://earthdoc.org/content/papers/10.3997/2214-4609.201700816)
- Kilhams, B., Chedburn, L., Schofield, N., Lunde, I.L., Romain, H., Jolley, D. and Eide, C.H. 2021. The spatial distribution of igneous centres along the Norwegian Atlantic Margin (Møre and Vøring) and their relationship to magmatic plumbing systems. *Journal of the Geological Society, London*, **175**, jgs2020-192, <https://doi.org/10.1144/jgs2020-192>
- Kilhams, B., Chedburn, L. et al. 2022. Challenges and opportunities for hydrocarbon exploration within the Mesozoic sub-basalt plays of the Norwegian Atlantic Margin. *Petroleum Geoscience*, **28**, <https://doi.org/10.1144/petgeo2022-022>
- Kinny, P.D., Friend, C.R.L. and Love, G.J. 2005. Proposal for a terrane-based nomenclature for the Lewisian Gneiss Complex of NW Scotland. *Journal of the Geological Society, London*, **162**, 175–186, <https://doi.org/10.1144/0016-764903-149>
- Kuszniir, N.J., Roberts, A.M. and Alvey, A.D. 2020. Crustal structure of the conjugate Equatorial Atlantic Margins, derived by gravity anomaly inversion. *Geological Society, London, Special Publications*, **476**, 83–107, <https://doi.org/10.1144/SP476.5>
- Lang, G., ten Brink, U.A., Hutchinson, D.R., Mountain, G.S. and Schattner, U. 2020. The role of premagmatic rifting in shaping a volcanic continental margin: an example from the eastern North American margin. *Journal of Geophysical Research: Solid Earth*, **125**, e2020JB019576, <https://doi.org/10.1029/2020JB019576>
- Larsen, M., Rasmussen, T. and Hjelm, L. 2010. Cretaceous revisited: exploring the syn-rift play of the Faroe–Shetland Basin. *Geological Society, London, Petroleum Geology Conference Series*, **7**, 953–962, <https://doi.org/10.1144/0070953>
- Layfield, L.K., Schofield, N. et al. 2022. New insights into the structure, geology and hydrocarbon prospectivity along the central-northern Corona Ridge, Faroe–Shetland Basin. *Petroleum Geoscience*, **28**, petgeo2021-090, <https://doi.org/10.1144/petgeo2021-090>
- Lyngsø, S.B. and Thybo, H. 2007. A new tectonic model for the Laurentia–Avalonia–Baltica sutures in the North Sea: a case study along MONA LISA profile 3. *Tectonophysics*, **429**, 201–227, <https://doi.org/10.1016/j.tecto.2006.09.017>
- MacLennan, J. and Lovell, B. 2002. Control of regional sea level by surface uplift and subsidence caused by magmatic underplating of Earth's crust. *Geology*, **30**, 675–678, [https://doi.org/10.1130/0091-7613\(2002\)030%3C0675:CORSLB%3E2.0.CO;2](https://doi.org/10.1130/0091-7613(2002)030%3C0675:CORSLB%3E2.0.CO;2)
- Magee, C., Stevenson, C.T.E. et al. 2018. Magma plumbing systems: a geophysical perspective. *Journal of Petrology*, **59**, 1217–1251, <https://doi.org/10.1093/ptrology/egy064>
- Makris, J., Papoulia, I. and Ziska, H. 2009. Crustal structure of the Shetland–Faeroe Basin from long offset seismic data. In: Ziska, H. and Varming, T. (eds) *Faroe Islands Exploration Conference: Proceedings of the 2nd Conference*. Faroese Society of Sciences and Humanities, Tórshavn, 30–42.
- Mark, N.J., Schofield, N. et al. 2018a. Overthickening of sedimentary sequences by igneous intrusions. *Journal of the Geological Society, London*, **176**, 46–60, <https://doi.org/10.1144/jgs2018-112>
- Mark, N.J., Schofield, N. et al. 2018b. Igneous intrusions in the Faroe Shetland basin and their implications for hydrocarbon exploration; new insights from well and seismic data. *Marine and Petroleum Geology*, **92**, 733–753, <https://doi.org/10.1016/j.marpetgeo.2017.12.005>
- McBride, J.H., White, R.S., Smallwood, J.R. and England, R.W. 2004. Must magmatic intrusion in the lower crust produce reflectivity? *Tectonophysics*, **388**, 271–297, <https://doi.org/10.1016/j.tecto.2004.07.055>
- McQuillin, R., Bacon, N. and Barclay, W. 1979. *An Introduction to Seismic Interpretation*. Graham & Trotman, London.
- Mjelde, R., Digranes, P. et al. 2001. Crustal structure of the outer Vøring Plateau, offshore Norway, from ocean bottom seismic and gravity data. *Journal of Geophysical Research*, **106**, 6769–6791, <https://doi.org/10.1029/2000JB900415>
- Mjelde, R., Faleide, J.I., Breivik, A.J. and Raum, T. 2009. Lower crustal composition and crustal lineaments on the Vøring Margin, NE Atlantic: a review. *Tectonophysics*, **472**, 183–193, <https://doi.org/10.1016/j.tecto.2008.04.018>
- Mjelde, R., Kvarven, T., Faleide, J.I. and Thybo, H. 2016. Lower crustal high-velocity bodies along North Atlantic passive margins, and their link to Caledonian suture zone eclogites and Early Cenozoic magmatism. *Tectonophysics*, **670**, 16–29, <https://doi.org/10.1016/j.tecto.2015.11.021>
- Moy, D.J. and Imber, J. 2009. A critical analysis of the structure and tectonic significance of rift-oblique lineaments ('transfer zones') in the Mesozoic–Cenozoic succession of the Faroe–Shetland Basin, NE Atlantic margin. *Journal of the Geological Society, London*, **166**, 831–844, <https://doi.org/10.1144/0016-76492009-010>
- Mudge, D.C. 2015. Regional controls on Lower Tertiary sandstone distribution in the North Sea and NE Atlantic margin basins. *Geological Society, London, Special Publications*, **403**, 17–42, <https://doi.org/10.1144/SP403.5>
- Nadin, P.A., Kuszniir, N.J. and Cheadle, M.J. 1997. Early Tertiary plume uplift of the North Sea and Faeroe–Shetland basins. *Earth and Planetary Science Letters*, **148**, 109–127, [https://doi.org/10.1016/S0012-821X\(97\)00035-6](https://doi.org/10.1016/S0012-821X(97)00035-6)
- Naylor, P.H., Bell, B.R., Jolley, D.W., Durnall, P. and Fredsted, R. 1999. Palaeogene magmatism in the Faeroe–Shetland Basin: influences on uplift history and sedimentation. *Geological Society, London, Petroleum Geology Conference Series*, **5**, 545–558, <https://doi.org/10.1144/0050545>
- North Sea Transition Authority (NSTA) 2022. *UK National Data Repository*, <https://ndr.nstauthority.co.uk/>
- Passy, S.R. and Bell, B.R. 2007. Morphologies and emplacement mechanisms of the lava flows of the Faroe Islands Basalt Group, Faroe Islands, NE Atlantic Ocean. *Bulletin of Volcanology*, **70**, 139–156, <https://doi.org/10.1007/s00445-007-0125-6>
- Passy, S. and Hitchen, K. 2011. Cenozoic (igneous). In: Ritchie, J.D., Ziska, H., Johnson, H. and Evans, D. (eds) *Geology of the Faroe–Shetland Basin and Adjacent Areas*. British Geological Survey, Nottingham, 209–228, <https://pubs.bgs.ac.uk/publications.html?pubID=B06836>
- Passy, S. and Jolley, D.W. 2009. A revised lithostratigraphic nomenclature for the Palaeogene Faroe Islands Basalt Group, NE Atlantic Ocean. *Earth and Environmental Science Transactions of the Royal Society of Edinburgh*, **99**, 127–158, <https://doi.org/10.1017/S1755691009008044>
- Peron-Pinvidic, G., Åkermoen, T. and Leivestad, L.I. 2022. The North-East Atlantic Mid-Norwegian rifted margin: insights from the deep imaging Geoex MCG RDH19 dataset. *Tectonophysics*, **824**, 229225, <https://doi.org/10.1016/j.tecto.2022.229225>
- Persano, C., Barfod, D.N., Stuart, F.M. and Bishop, P. 2007. Constraints on early Cenozoic underplating-driven uplift and denudation of western Scotland from low temperature thermochronometry. *Earth and Planetary Science Letters*, **263**, 404–419, <https://doi.org/10.1016/j.epsl.2007.09.016>
- Petersen, U.K. and Funck, T. 2017. Review of velocity models in the Faroe–Shetland Channel. *Geological Society, London, Special Publications*, **447**, 833–844, <https://doi.org/10.1144/SP447.7>
- PGS Imaging 2016. *Full Integrity PreSTM Processing Report*. North Sea Transition Authority UK National Data Repository **269636169**, <https://ndr.nstauthority.co.uk/>
- Planke, S., Rasmussen, T., Rey, S.S. and Myklebusy, R. 2005. Seismic characteristics and distribution of volcanic intrusions and hydrothermal vent complexes in the Vøring and Møre basins. *Geological Society, London, Petroleum Geology Conference Series*, **6**, 947–956, <https://doi.org/10.1144/0060833>
- Poppitt, S., Duncan, L.J., Preu, B., Fazzari, F. and Archer, J. 2018. The influence of volcanic rocks on the characterization of Rosebank Field – new insights from ocean-bottom seismic data and geological analogues integrated through interpretation and modelling. *Geological Society, London, Petroleum Geology Conference Series*, **8**, 373–384, <https://doi.org/10.1144/PGC8.6>
- Quinn, M. and Ziska, H. 2011. Structure. In: Ritchie, J.D., Ziska, H., Johnson, H. and Evans, D. (eds) *Geology of the Faroe–Shetland Basin and Adjacent Areas*. British Geological Survey, Nottingham, <https://pubs.bgs.ac.uk/publications.html?pubID=B06836>
- Raum, T., Mjelde, R. et al. 2005. Sub-basalt structures east of the Faroe Islands revealed from wide-angle seismic and gravity data. *Petroleum Geoscience*, **11**, 291–308, <https://doi.org/10.1144/1354-079304-627>
- Reston, T.J. 1988. Evidence for shear zones in the lower crust offshore Britain. *Tectonics*, **7**, 929–945, <https://doi.org/10.1029/TC007i005p00929>
- Richardson, K.R., Smallwood, J.R., White, R.S., Snyder, D.B. and Maguire, P.K.H. 1998. Crustal structure beneath the Faroe Islands and the Faroe–Iceland Ridge. *Tectonophysics*, **300**, 159–180, [https://doi.org/10.1016/S0040-1951\(98\)00239-X](https://doi.org/10.1016/S0040-1951(98)00239-X)
- Ripington, S., Mazur, S. and Warner, J. 2015. The crustal architecture of the Faroe–Shetland Basin: insights from a newly merged gravity and magnetic dataset. *Geological Society, London, Special Publications*, **421**, 169–196, <https://doi.org/10.1144/SP421.10>
- Ritchie, J.D., Johnson, H., Quinn, M.F. and Gatiliff, R.W. 2008. The effects of Cenozoic compression within the Faroe–Shetland Basin and adjacent areas. *Geological Society, London, Special Publications*, **306**, 121–136, <https://doi.org/10.1144/SP306.5>
- Ritchie, J.D. and Varming, T. 2011. Jurassic. In: Ritchie, J.D., Ziska, H., Johnson, H. and Evans, D. (eds) *Geology of the Faroe–Shetland Basin and Adjacent Areas*. British Geological Survey, Nottingham, 103–123, <https://pubs.bgs.ac.uk/publications.html?pubID=B06836>

- Ritchie, J.D., Ziska, H., Kimbell, G., Quinn, M. and Chadwick, A. 2011. Structure. In: Ritchie, J.D., Ziska, H., Johnson, H. and Evans, D. (eds) *Geology of the Faroe-Shetland Basin and Adjacent Areas*. British Geological Survey, Nottingham, 9–70, <https://pubs.bgs.ac.uk/publications.html?pubID=B06836>
- Ritter, U., Zielinski, G.W., Weiss, H.M., Zielinski, R.L.B. and Sættem, J. 2004. Heat flow in the Vøring Basin, Mid-Norwegian Shelf. *Petroleum Geoscience*, **4**, 353–365, <https://doi.org/10.1144/1354-079303-616>
- Roberts, A.W., White, R.S. and Christie, P.A.F. 2009. Imaging igneous rocks on the North Atlantic rifted continental margin. *Geophysical Journal International*, **179**, 1024–1038, <https://doi.org/10.1111/j.1365-246X.2009.04306.x>
- Roberts, A.M., Alvey, A.D. and Kusznir, N.J. 2020. Crustal structure and heat-flow history in the UK Rockall Basin, derived from backstripping and gravity-inversion analysis. *Petroleum Geoscience*, **25**, 131–150, <https://doi.org/10.1144/petgeo2017-063>
- Rudge, J.F., Shaw Champion, M.E., White, N., McKenzie, D. and Lovell, B. 2008. A plume model of transient diachronous uplift at the Earth's surface. *Earth and Planetary Science Letters*, **267**, 146–160, <https://doi.org/10.1016/j.epsl.2007.11.040>
- Schofield, N., Holford, S. *et al.* 2017. Regional magma plumbing and emplacement mechanisms of the Faroe–Shetland Sill Complex: implications for magma transport and petroleum systems within sedimentary basins. *Basin Research*, **29**, 41–63, <https://doi.org/10.1111/bre.12164>
- Shaw-Champion, M.E., White, N.J., Jones, S.M. and Priestley, K.F. 2006. Crustal velocity structure of the British Isles; a comparison of receiver functions and wide-angle seismic data. *Geophysical Journal International*, **166**, 795–813, <https://doi.org/10.1111/j.1365-246X.2006.03050.x>
- Shaw-Champion, M.E., White, N.J., Jones, S.M. and Lovell, J.P.B. 2008. Quantifying transient mantle convective uplift: an example from the Faroe–Shetland basin. *Tectonics*, **27**, TC1002, <https://doi.org/10.1029/2007TC002106>
- Sheriff, R.E. and Geldart, L.P. 1982. *Exploration Seismology*. Cambridge University Press, Cambridge.
- Smallwood, J.R. 2004. Tertiary inversion in the Faroe–Shetland Channel and the development of major erosional scarps. *Geological Society, London, Memoirs*, **29**, 187–198, <https://doi.org/10.1144/GSL.MEM.2004.029.01.18>
- Smallwood, J.R. 2008. Uplift, compression and the Cenozoic Faroe–Shetland sediment budget. *Geological Society, London, Special Publications*, **306**, 137–152, <https://doi.org/10.1144/SP306.6>
- Smallwood, J.R. and Gill, C.E. 2002. The rise and fall of the Faroe–Shetland Basin: evidence from seismic mapping of the Balder Formation. *Journal of the Geological Society, London*, **159**, 627–630, <https://doi.org/10.1144/0016-764902-064>
- Smallwood, J.R. and Maresh, J. 2002. The properties, morphology and distribution of igneous sills: modelling, borehole data and 3D seismic from the Faroe–Shetland area. *Geological Society, London, Special Publications*, **197**, 271–306, <https://doi.org/10.1144/GSL.SP.2002.197.01.11>
- Smallwood, J.R., Staples, R.K., Richardson, R. and White, R.S. 1999. Crust generated above the Iceland mantle plume: from continental rift to oceanic spreading center. *Journal of Geophysical Research*, **101**, 22885–22902, <https://doi.org/10.1029/1999JB900176>
- Smith, K. and Ziska, H. 2011. Devonian and Carboniferous. In: Ritchie, J.D., Ziska, H., Johnson, H. and Evans, D. (eds) *Geology of the Faroe–Shetland Basin and Adjacent Areas*. British Geological Survey, Nottingham, 79–91, <https://pubs.bgs.ac.uk/publications.html?pubID=B06836>
- Smith, L.K., White, R.S., Kusznir, N.J. and iSIMM Team 2005. Structure of the Hatton Basin and adjacent continental margin. *Geological Society, London, Petroleum Geology Conference Series*, **6**, 947–956, <https://doi.org/10.1144/0060947>
- Sørensen, A.B. 2003. Cenozoic basin development and stratigraphy of the Feroes area. *Petroleum Geoscience*, **9**, 189–207, <https://doi.org/10.1144/1354-079302-508>
- Stoker, M.S. 2016. Cretaceous tectonostratigraphy of the Faroe–Shetland region. *Scottish Journal of Geology*, **52**, 19–41, <https://doi.org/10.1144/sjg2016-004>
- Stoker, M.S. and Ziska, H. 2011. Cretaceous. In: Ritchie, J.D., Ziska, H., Johnson, H. and Evans, D. (eds) *Geology of the Faroe–Shetland Basin and Adjacent Areas*. British Geological Survey, Keyworth, Nottingham, 123–150, <https://pubs.bgs.ac.uk/publications.html?pubID=B06836>
- Stoker, M.S., Holford, S.P., Hillis, R.R., Green, P.F. and Duddy, I.R. 2010. Cenozoic post-rift sedimentation off northwest Britain: recording the detritus of episodic uplift on a passive continental margin. *Geology*, **38**, 595–598, <https://doi.org/10.1130/G30881.1>
- Stoker, M., Doornenbal, H., Hopper, J.R. and Gaina, C. 2014. Tectonostratigraphy. In: Hopper, J.R., Funck, T., Stoker, M., Årting, U., Peron-Pinvidic, G., Doornenbal, H. and Gaina, C. (eds) *Tectonostratigraphic Atlas of the North-East Atlantic Region*. Geological Survey of Denmark and Greenland, Copenhagen.
- Stoker, M.S., Holford, S.P. and Hillis, R.R. 2017a. A rift-to-drift record of vertical crustal motions in the Faroe–Shetland Basin, NW European margin: establishing constraints on NE Atlantic evolution. *Journal of the Geological Society, London*, **175**, 263–274, <https://doi.org/10.1144/jgs2017-076>
- Stoker, M.S., Stewart, M.A. *et al.* 2017b. An overview of the Upper Palaeozoic–Mesozoic stratigraphy of the NE Atlantic region. *Geological Society, London, Special Publications*, **447**, 11–68, <https://doi.org/10.1144/SP447.2>
- Thybo, H. and Artemieva, I.M. 2013. Moho and magmatic underplating in continental lithosphere. *Tectonophysics*, **609**, 605–619, <https://doi.org/10.1016/j.tecto.2013.05.032>
- Thybo, H., Artemieva, I.M. and Kennett, B. 2013. Moho: 100 years after Andrija Mohorovičić. *Tectonophysics*, **609**, 1–8, <https://doi.org/10.1016/j.tecto.2013.10.004>
- Tiley, R., White, N. and Al-Kindi, S. 2004. Linking Paleogene denudation and magmatic underplating beneath the British Isles. *Geological Magazine*, **141**, 345–351, <https://doi.org/10.1017/S0016756804009197>
- Trude, K.J. 2004. Kinematic indicators for shallow level igneous intrusions from 3D seismic data: evidence of flow direction and feeder location. *Geological Society, London, Memoirs*, **29**, 209–218, <https://doi.org/10.1144/GSL.MEM.2004.029.01.20>
- Walker, F., Schofield, N. *et al.* 2021. Inside the volcano: three-dimensional magmatic architecture of a buried shield volcano. *Geology*, **49**, 243–247, <https://doi.org/10.1130/G47941.1>
- Wangen, M., Mjelde, R. and Faleide, J.I. 2011. The extension of the Vøring margin (NE Atlantic) in case of differing degrees of magmatic underplating. *Basin Research*, **23**, 83–100, <https://doi.org/10.1111/j.1365-2117.2010.00467.x>
- Warner, M.R. 1987. Seismic reflections from the Moho – the effect of isostasy. *Geophysical Journal of the Royal Astronomical Society*, **88**, 425–435, <https://doi.org/10.1111/j.1365-246X.1987.tb06651.x>
- Warner, M. 1990. Absolute reflection coefficients from deep seismic reflections. *Tectonophysics*, **173**, 15–23, [https://doi.org/10.1016/0040-1951\(90\)90199-1](https://doi.org/10.1016/0040-1951(90)90199-1)
- Watson, D., Schofield, N. *et al.* 2017. Stratigraphic overview of Palaeogene tuffs in the Faroe–Shetland Basin, NE Atlantic Margin. *Journal of the Geological Society*, **174**, 627–645, <https://doi.org/10.1144/jgs2016-132>
- White, N. and Lovell, B. 1997. Measuring the pulse of a plume with the sedimentary record. *Nature*, **387**, 888–891, <https://doi.org/10.1038/43151>
- White, R.S. 1992. Crustal structure and magmatism of North Atlantic continental margins. *Journal of the Geological Society, London*, **149**, 841–854, <https://doi.org/10.1144/gsjgs.149.5.0841>
- White, R.S. 1997. Rift-plume interaction in the North Atlantic. *Philosophical Transactions of the Royal Society of London Series A*, **355**, 319–338, <https://doi.org/10.1098/rsta.1997.0011>
- White, R.S. and McKenzie, D.P. 1989a. Volcanism at rifts. *Scientific American*, **261**, 62–71, <https://doi.org/10.1038/SCIENTIFICAMERICAN0789-62>
- White, R.S. and McKenzie, D.P. 1989b. Magmatism at rift zones: the generation of volcanic continental margins and flood basalts. *Journal of Geophysical Research*, **94**, 7685–7729, <https://doi.org/10.1029/JB094iB06p07685>
- White, R.S. and Smith, L.K. 2009. Crustal structure of the Hatton and the conjugate east Greenland rifted volcanic continental margins, NE Atlantic. *Journal of Geophysical Research*, **114**, <https://doi.org/10.1029/2008JB005856>
- White, R.S., Spence, G.D., Fowler, S.R., McKenzie, D.P., Westbrook, G.K. and Bowen, A.N. 1987. Magmatism at rifted continental margins. *Nature*, **330**, 439–444, <https://doi.org/10.1038/330439a0>
- White, R.S., Christie, P.A.F. *et al.* 2002. iSIMM pushes frontiers of marine seismic acquisition. *First Break*, **20**, 782–786.
- White, R.S., Spitzer, R., Christie, P.A.F., Roberts, A., Lunnon, Z., Maresh, J. and iSIMM Working Group 2005. Seismic imaging through basalt flows on the Feroes Shelf. In: Ziska, H., Varming, T. and Blotch, D. (eds) *Faroe Islands Exploration Conference: Proceedings of the 1st Conference*. Faroese Society of Sciences and Humanities, Tórshavn, 11–31.
- White, R.S., Smith, L.K., Roberts, A.W., Christie, P.A.F., Kusznir, N. and Team iSIMM 2008. Lower-crustal intrusion on the north Atlantic continental margin. *Nature*, **452**, 460–464, <https://doi.org/10.1038/nature06687>
- White, R.S., Eccles, J.D. and Roberts, A.W. 2010. Constraints on volcanism, igneous intrusion and stretching on the Rockall–Faroe continental margin. *Geological Society, London, Petroleum Geology Conference Series*, **7**, 831–842, <https://doi.org/10.1144/0070831>
- Wrona, T., Fossen, H., Lecomte, I., Eide, C.H. and Gawthorpe, R.L. 2019a. Seismic expression of shear zones: insights from 2-D point-spread-function based convolution modelling. *Journal of Structural Geology*, **140**, 104121, <https://doi.org/10.1016/j.jsg.2020.104121>
- Wrona, T., Magee, C., Fossen, H., Gawthorpe, R.L., Bell, R.E., Jackson, C.A.-L. and Faleide, J.I. 2019b. 3-D seismic images of an extensive igneous sill in the lower crust. *Geology*, **47**, 729–733, <https://doi.org/10.1130/G46150.1>
- Xu, W., Huang, S. *et al.* 2021. Geothermal gradient and heat flow of the Erlian Basin and adjacent areas, northern China: geodynamic implication. *Geothermics*, **92**, <https://doi.org/10.1016/j.geothermics.2021.102049>